10448–10464 *Nucleic Acids Research, 2021, Vol. 49, No. 18* *Published online 27 September 2021*
https://doi.org/10.1093/nar/gkab844

Fusarium BP1 is a reader of H3K27 methylation

Guangfei Tang[1,2,†], Jianlong Yuan[3,†], Jing Wang[1], Yi-Zhe Zhang[3], Si-Si Xie[3], Hongkai Wang[1], Zeng Tao[1], Huiquan Liu[4], H. Corby Kistler[5], Youfu Zhao[6], Cheng-Guo Duan[3], Wende Liu[2,*], Zhonghua Ma[1,*] and Yun Chen[1,*]

[1]State Key Laboratory of Rice Biology, Key Laboratory of Molecular Biology of Crop Pathogens and Insects, Institute of Biotechnology, Zhejiang University, Hangzhou 310058, China, [2]State Key Laboratory for Biology of Plant Diseases and Insect Pests, Institute of Plant Protection, Chinese Academy of Agricultural Sciences, Beijing 100193, China, [3]Shanghai Center for Plant Stress Biology and CAS Center for Excellence in Molecular Plant Sciences, Chinese Academy of Sciences, Shanghai 201602, China, [4]State Key Laboratory of Crop Stress Biology for Arid Areas and NWAFU-Purdue Joint Research Center, Northwest A&F University, Yangling 712100, China, [5]Cereal Disease Laboratory, Agricultural Research Service, United States Department of Agriculture, Saint Paul, MN 55108, USA and [6]Department of Crop Sciences, University of Illinois at Urbana-Champaign, Urbana, IL 61801, USA

Received October 03, 2020; Revised August 31, 2021; Editorial Decision September 07, 2021; Accepted September 10, 2021

ABSTRACT

Histone H3 lysine 27 methylation catalyzed by polycomb repressive complex 2 (PRC2) is conserved from fungi to humans and represses gene transcription. However, the mechanism for recognition of methylated H3K27 remains unclear, especially in fungi. Here, we found that the bromo-adjacent homology (BAH)-plant homeodomain (PHD) domain containing protein BAH–PHD protein 1 (BP1) is a reader of H3K27 methylation in the cereal fungal pathogen *Fusarium graminearum*. BP1 interacts with the core PRC2 component Suz12 and directly binds methylated H3K27. BP1 is distributed in a subset of genomic regions marked by H3K27me3 and represses gene transcription. The BP1 deletion mutant shows identical phenotypes on mycelial growth and virulence, as well as similar expression profiles of secondary metabolite genes to the strain lacking the H3K27 methyltransferase Kmt6. More importantly, BP1 can directly bind DNA through its PHD finger, which might increase nucleosome residence and subsequently reinforce transcriptional repression in H3K27me3-marked target regions. A phylogenetic analysis showed that BP1 orthologs are mainly conserved in fungi. Overall, our findings provide novel insights into the mechanism by which PRC2 mediates gene repression in fungi, which is distinct from the PRC1-PRC2 system in plants and mammals.

INTRODUCTION

The establishment and maintenance of chromatin structure is critical for the development and environmental adaptation of eukaryotes. Reversible epigenetic histone modifications can alter chromatin structure to tightly regulate gene expression (1,2). Polycomb repressive complex-2 (PRC2) catalyzes the methylation of lysine residue K27 in histone 3 (H3K27) methylation, resulting in facultative heterochromatin for transcriptional repression at Polycomb target loci (3). PRC2 was originally discovered in *Drosophila melanogaster*, and is evolutionarily conserved in organisms ranging from fungi to humans (4,5). In *Drosophila*, PRC2 is formed by four core proteins: enhancer of zeste E(Z), suppressor of zeste 12 SU(Z)12, extra sex combs (ESC) and the Nurf55 protein. The E(Z) protein contains a SET domain and exerts histone lysine methyltransferase (HMT) activity for trimethylating H3K27 (H3K27me3). Su(z)12 and Nurf55 compose the nucleosome-binding subunits in PRC2 and anchor the E(z) enzyme onto chromatin substrates, and ESC is required for HMT activity enhancement (6). Increasing data indicate that variant forms of PRC2 with distinct components and accessory proteins exist in plants and animals; however, the assembly of fungal PRC2 is less understood (7).

Precise recognition of histone epigenetic marks by 'reader' proteins is essential for establishing and maintaining proper chromatin structure and gene expression. H3K27me3 deposited by PRC2 is classically recognized by another Polycomb repressive complex PRC1, which participates in PRC2 recruitment and promotes chromatin compaction for gene silencing in animals and

*To whom correspondence should be addressed. Tel: +86 571 8898 2106; Email: chenyun0927@zju.edu.cn
Correspondence may also be addressed to Wende Liu. Email: wdliu@ippcaas.cn
Correspondence may also be addressed to Zhonghua Ma. Email: zhma@zju.edu.cn
†The authors wish it to be known that, in their opinion, the first two authors should be regarded as Joint First Authors.

plants (8–10). H3K27me3 is read by PRC1 through chromodomain (ChD)-containing chromobox homolog (CBX) proteins in animals (11). In plants, LHP1 interacts with the Nurf55 homolog, MSI1, directly binds H3K27me3 and forms a positive feedback loop to recruit PRC2 (12,13). EMBRYONIC FLOWER 1 (EMF1) is another component of PRC1 in *Arabidopsis* and is proposed to mediate H3K27me3-dependent gene silencing through chromatin compaction (14). Moreover, variant PRC1 can ubiquitylate histone H2A by RING1A/B to positively regulate PRC2 in both plant and animal systems (5,15,16). In addition to PRC1, many specific domain-containing proteins have been found to be involved in H3K27me3 'read out' (17,18). For example, the Tudor domain in PHF1 and the bromo-adjacent homology (BAH) domain in the BAHD1 protein can directly bind H3K27me3 to stimulate PRC2 activity in mammals (19–21). The BAH and plant homeodomain (PHD) finger-containing proteins SHL and EBS read H3K27me3 and regulate the growth and floral phase transition of flowering plants (22–24).

PRC2 is well conserved in many fungi; however, components of PRC1 are notably absent in this kingdom (7). This absence implies that unidentified reader proteins may recognize H3K27 methylation in fungi. Thus, identification and characterization of a fungal PRC2 reader is critical for understanding how fungi maintain gene repression and may also reveal general mechanisms by which PRC2 regulates gene expression in higher eukaryotes. In this study, we identified a PRC2-interacting protein in the cereal fungal pathogen *Fusarium graminearum*, which contains a BAH domain and PHD finger and was designated as BP1 (BAH-PHD protein 1). BP1 localizes to the nucleus and directly interacts with the Suz12 component of PRC2 in a BAH and PHD finger-dependent manner. More importantly, in contrast to the H3K27 methylation recognition system that depends on PRC1 in plants and animals, BP1 can bind methylated H3K27 peptides and exhibits DNA-binding activity at PRC2 target loci. The results of this study indicate that BP1 is a reader of H3K27 methylation in fungi, which provides novel insight into the regulatory mechanism of PRC2 in gene transcriptional repression.

MATERIALS AND METHODS

Fungal strains and culture conditions

The *F. graminearum* wild-type strain PH-1 (NRRL 31084) was used as a parental strain for transformants generated in this study. The wild-type and transformant strains were grown on potato dextrose agar (PDA) (200 g potato, 20 g glucose, 10 g agar and 1 l water) for growth rate examination. Mycelia grown in yeast extract peptone dextrose (YEPD) medium (10 g peptone, 3 g yeast extract, 20 g D-glucose and 1 l water) were used for ChIP-seq and ChIP-qPCR.

Strain construction

The Δ*Kmt6*, Δ*Eed*, Δ*Suz12* and Δ*BP1* gene deletion mutants were generated by the double-joint PCR approach (25). Polyethylene glycol (PEG)-mediated protoplast transformation of *F. graminearum* was carried out using protocols described previously (26). Briefly, the open reading frame (ORF) of each gene was replaced with a hygromycin (HPH) resistance cassette, and the resulting deletion mutants were identified by PCR assays with the relevant primers (Supplementary Table S1). For Δ*Kmt6* complementation, the fragment containing the native promoter and ORF (without stop codon) of Kmt6 was amplified with the relevant primers. The resulting PCR products were purified and then co-transformed with the XhoI-digested pYF11-gfp-G418 plasmid into the yeast strain XK1-25 using the Alkali-Cation Yeast Transformation Kit (MP Biomedicals, Solon, USA) to generate a recombinant vector, pYF11-KMT6-gfp. Subsequently, the pYF11-KMT6-gfp vector was recovered from the yeast transformant by using the yeast plasmid extract kit (Solarbio, Beijing, China) and then transferred into *Escherichia coli* strain DH5α for propagation. The recombinant plasmid pYF11-KMT6-gfp was purified from *E. coli* and introduced into Δ*Kmt6* to generate the complementation strain Δ*Kmt6*-C (Δ*Kmt6*::Kmt6-GFP). Transformants were selected with geneticin (G418). The Eed-GFP, Suz12-GFP, BP1-GFP and BP1-mCherry fusion constructs were similarly constructed.

To construct the truncated proteins $BP1^{\Delta BAH}$ and $BP1^{\Delta PHD}$, PH-1 genomic DNA was used as a template for amplifying the corresponding fragments. To generate the $BP1^{\Delta BAH}$-GFP strain, the upstream fragment of the BAH domain (1858 bp, including the native promoter) and downstream fragment of BAH domain (652 bp, without stop codon) were amplified with the primers P51/52, and P53/54, respectively. These two fragments were fused by double-joint PCR and then co-transformed with the XhoI-digested pYF11-gfp-G418 plasmid into the yeast strain XK1-25. Then, the recombinant plasmid pYF11-$BP1^{\Delta BAH}$-gfp-G418 was transformed into ΔBP1 to generate $BP1^{\Delta BAH}$-GFP strain. The $BP1^{\Delta PHD}$-GFP, $BP1^{\Delta BAH}$-mCherry, and $BP1^{\Delta PHD}$-mCherry strains were similarly constructed.

To construct the Δ*BP1*::EBS-C (Δ*BP1*::EBS-GFP), Δ*BP1*::SHL-C (Δ*BP1*::SHL-GFP) and Δ*BP1*::EPR1-C (Δ*BP1*::EPR1-GFP) heterogeneous complementation strains, the fragments containing the promoter (BP1) region and open reading frame (EBS, SHL or EPR1, without stop codon) were amplified and fused by overlapping PCR. The resulting fused fragments were subsequently co-transformed with the XhoI-digested pYF11-gfp-G418 plasmid into the yeast strain XK1-25. The recombinant plasmid was individually introduced into Δ*BP1*, and then the resulting transformants were identified by PCR assays with the relevant primers (Supplementary Table S1). Before protoplast transformation, all recombinant plasmids were verified by DNA sequencing.

Microscopic observations

For observation of the localization of fluorescent fusion proteins, each strain was cultured in potato dextrose broth (PDB) at 25°C for 24 h, and fresh mycelia were examined with a Zeiss LSM780 confocal microscope (Gottingen, Niedersachsen, Germany). To observe nuclei, fresh mycelia were washed with sterilized water and stained with

10 μg ml^{-1} 4′,6-diamidino-2-phenylindole (DAPI, Sigma). The following excitation/emission UV wavelengths were used for fluorescent detection: DAPI, 405/410–470 nm; mCherry, 561/590–640 nm; GFP, 488/490–530 nm.

Affinity capture-mass spectrometry (ACMS) analysis

Fresh mycelia (2.0 g) of the Δ*Kmt6*::Kmt6-Flag strain were finely ground and suspended in 10 ml of extraction buffer (50 mM Tris–HCl, pH 7.5, 100 mM NaCl, 5 mM EDTA, 1% Triton X-100, 2 mM phenylmethylsulfonyl fluoride) supplemented with 100 μl of protease inhibitor cocktail (phenylmethanesulfonyl fluoride, 100 mM; pepstatin A, 2.2 mM; L-*trans*-epoxysuccinyl-leucylamido (4-guanidino) butane, 1.4 mM; 1,10-phenanthroline, 500 mM) (C600382, Sangon Co., Shanghai, China). After centrifugation at 10 000 g for 20 min at 4°C, supernatant (8 ml) was transferred into a sterilized tube. Approximately 250 μl of anti-Flag agarose (M20018S, Abmart, Shanghai, China) was added to capture Kmt6-Flag interacting proteins following the manufacturer's instructions. After incubation at 4°C overnight, agarose was washed three times with 2.5 ml of Tris buffered saline (TBS, 20 mM Tris–HCl, 500 mM NaCl, pH 7.5). Proteins binding to the beads were boiled with 600 μl TBS supplemented with 100 μl 10% SDS. After centrifugation at 5000 g for 5 min, proteins in the supernatant were concentrated to 70 μl and digested with trypsin as described previously (27). Tryptic peptides were analyzed by mass spectrometry (MS) by Shanghai Applied Protein Technology Co. Ltd (Shanghai, China). The Eed-GFP, Suz12-GFP and BP1-GFP interacting proteins were similarly captured by anti-GFP agarose (gta-20, ChromoTek, Martinsried, Germany), and MS analysis was performed. Three biological replicates were conducted for each protein.

Liquid chromatography electrospray ionization tandem mass spectrometry (LC–ESI-MS/MS) analysis

LC–MS/MS analysis was performed on a Q Exactive mass spectrometer coupled to Easy nLC (Thermo Fisher Scientific). The peptide mixture was loaded onto a reverse-phase trap column (Thermo Scientific Acclaim PepMap100, 100 μm × 2 cm, nanoViper C18) connected to a C18 reversed-phase analytical column (Thermo Scientific Easy Column, 75 μm × 10 cm, 3 μm resin) in buffer A (0.1% formic acid) and separated with a linear gradient of buffer B (84% acetonitrile and 0.1% formic acid) for 60 min at a flow rate of 300 nl/min controlled by IntelliFlow technology. Then, the peptides were injected into the Velos via ESI in positive ionization mode. MS data were acquired by choosing the most abundant precursor ions from the survey scan (300–1800 m/z) for higher-energy collision dissociation (HCD) fragmentation. The full MS1 scan was acquired at a resolution of 70 000 at 200 m/z. The automatic gain control target was set to 1 × 106 charges with a 40 ms maximum ion injection time. The dynamic exclusion duration was 30 s. The subsequent MS2 scan was set to 17 500 resolution at 200 m/z for HCD spectra, isolation width was 2 m/z, and maximum ion injection time was 50 ms. The normalized collision energy was 27 eV and the underfill ratio was defined as 0.1%.

MS/MS spectra were searched using the MASCOT engine (Matrix Science, London, UK; version 2.4) embedded in Proteome Discoverer 2.4 (Thermo Electron, San Jose, CA.) against the *F. graminearum* database https://fungidb.org/fungidb/app/downloads/Current_Release/FgraminearumPH-1/fasta/data/). An initial search was set at a precursor mass window of 6 ppm. The search followed an enzymatic cleavage rule of trypsin/P and allowed two maximal missed cleavage sites and a mass tolerance of 20 ppm for fragment ions. The database search was conducted according to the following parameters: carbamidomethylated cysteine was regarded as a fixed modification, while methionine oxidation was considered a variable modification. The cutoff of the global false discovery rate for peptide and protein identification was set to 0.01, and at least one unique peptide could be subjected to further quantification.

Western blotting analysis

Protein isolation was performed as previously described (26). The resulting proteins were separated by 10% SDS polyacrylamide gel electrophoresis (SDS-PAGE) and transferred onto an Immobilon-P transfer membrane (Millipore, Billerica, MA, USA). Monoclonal anti-GFP (ab32146, Abcam, Cambridge, UK), anti-mCherry (ab125096), anti-H3K4me3 (ab8580), anti-H3K36me3 (61102, Active Motif), anti-H3K27me3 (39155, Active Motif) and anti-Flag (SL5142, Sigma, Burlington, USA) antibodies were used for immunoblot analyses. Samples were also detected with monoclonal anti-GAPDH antibody (EM1101, Huanan Biotechnology Co., Ltd, Hangzhou, Zhejiang, China) or anti-H3 antibody (M130918, Huanan Biotechnology Co., Ltd, Hangzhou, Zhejiang, China) as a control. Three biological replicates were conducted for each experiment.

Co-immunoprecipitation (Co-IP) assays

For Co-IP assays, total proteins were extracted from dual-labeled (GFP and Flag tags) strains and incubated with anti-GFP-Trap® (gta-20, ChromoTek, Martinsried, Germany) agarose as described previously (28). Proteins eluted from agarose were analyzed by western blot with an anti-Flag and anti-GFP antibody. The protein samples were also detected with monoclonal anti-GAPDH antibody as a reference. Two biological replicates were conducted for each experiment.

Yeast two-hybrid assays

Y2H assays were performed according to the BD Matchmaker Library Construction & Screening Kits instructions (Clontech, PaloAlto, CA). Yeast two-hybrid (Y2H) assays were performed according to the BD Matchmaker Library Construction & Screening Kits instructions (Clontech, PaloAlto, CA). The full length ORF of each candidate gene was amplified using PH-1 genomic cDNA as the template, and cloned into the bait plasmids pGBKT7 and pGADT7, respectively. To construct the BP1$^{\Delta BAH}$ cassette for Y2H, the upstream fragment from the start codon to 291 bp in the ORF of BP1 and the downstream fragment

(450 bp from the end of the BAH domain to the last nucleotide before the stop codon) were amplified using PH-1 genomic cDNA as a template with the relevant primers. The purified PCR fragments were fused by double-joint PCR and subsequently cloned into pGBKT7 to generate pGBKT7-BP1$^{\Delta BAH}$. The pGBKT7-BP1$^{\Delta PHD}$ recombinant plasmid was similarly constructed. All recombinant plasmids were verified by sequencing before the Y2H assay to confirm that the inserted coding regions were correct without base shifts and mutation.

The resulting bait vector and each prey vector were co-transformed into *S. cerevisiae* strain Y2H Gold following the LiAc/ss-DNA/PEG (lithium acetate/single- stranded DNA/polyethylene glycol) transformation protocol. In addition, a pair of plasmids pGBKT7-53 and pGADT7 served as a positive control. A pair of plasmids pGBKT7-Lam and pGADT7 was used as a negative control. Serial concentrations of transformants were assayed for growth at 30°C for 3 days on basal medium SD (-Trp-Leu, without tryptophan and leucine), selective medium SD (-Trp-Leu-His, without tryptophan, leucine and histidine), and selective medium SD (-Trp-Leu-His-Ade, without tryptophan, leucine, histidine and adenine). Three independent experiments were performed to confirm yeast two-hybrid assay results (29).

Protein expression and purification

BP1 was amplified using PH-1 genomic cDNA, and then cloned into the pGEX-4T-1 vector (GST-tag) for peptide pull-down assays, pMAL-c2X vector (MBP-tag) for ITC and EMSA assays, and pET-22a vector (6 × His-tag) for bio-layer interferometry (BLI) assays. The plasmid was transformed into *E. coli* strain BL21 (DE3), and the cells were cultured in Luria Bertani medium containing 50 μg ml^{-1} ampicillin. Protein expression was induced by adding isopropyl β-D-thiogalactoside (IPTG) to a final concentration of 0.2 mM at 16°C, when the cell culture reached an optimal density at 600 nm of 0.4–0.6 at 37°C in a shaker. After an additional 10 h of culture, bacteria were harvested at 3990 rcf, at 4°C for 15 min. The bacterial pellet was resuspended in lysis buffer containing 200 mM NaCl, 20 mM MES pH 6.5, and 5% glycerol and disrupted by crushing at 800 bar at 4°C for 3 times. The disrupted homogenate was further processed by centrifugation at 11 860 rcf, at 4°C for 60 mins and the supernatant was transferred for FPLC system purification. The supernatant containing fusion GST tag protein was applied on a prepacked glutathione-Sepharose column (GST Trap High performance, GE Healthcare) by FPLC with a 1 ml/min flow rate. In the washing steps, the GST Trap column was washed with lysis buffer until the absorbance at 280 nm UV became stable. Finally, the proteins were eluted with lysis buffer plus 20 mM reduced L-glutathione (GSH). The eluted proteins were further purified by cation exchange chromatography (Heparin, HP, GE Healthcare). After sample application and washing, the elution step adopted a linearized model by gradually increasing the salt concentration to 1 M NaCl in 50 min. During this process, the target proteins were gradually eluted and fractionized to 96-well deep plates with 1.8 ml elute in each well. The fractions corresponding to the elution curve (absorbance curve of UV 280 nm) were subjected to SDS-PAGE analysis. Finally, the target proteins were concentrated to less than 2 ml and subjected to size exclusion chromatography (SEC), and the elution peak corresponding to the monomeric state of the target proteins was concentrated for subsequent experiments. The fusion MBP and 6× His-tagged proteins were purified by the same strategy as GST fusion proteins, except for in the capture steps. The MBP and His trap FF column (GE, Healthcare) was adopted, and lysis buffer plus 20 mM maltose or 500 mM imidazole was used as the elution buffer for eluting MBP and His-tag fusion protein, respectively.

The GST-BP1$^{\Delta BAH}$, GST-BP1$^{\Delta PHD}$, MBP-BP1$^{\Delta BAH}$ and MBP-BP1$^{\Delta PHD}$ were similarly cloned, expressed and purified as described above. All of the mutations were generated by a double-joint PCR approach and were expressed and purified using the same protocol used for the full-length protein. Purified and desalted proteins were stored at −80°C for future use.

Peptide pull-down

Peptide pull-down assays were performed as follows: 1.5 μg of biotinylated histone peptides were first incubated with 62.5 μl of magnetic streptavidin beads (S1420S, NEB, New England Biolabs) in 1 ml of peptide binding buffer (50 mM Tris−HCl, pH 8.0, 300 mM NaCl, 0.1% NP-40) for 1 h at 4°C. Then, peptide-bound beads were washed twice with 1 ml of peptide binding buffer, and then incubated with 1.5 μg of GST-tagged full-length or truncated BP1 proteins in 0.5 ml of binding buffer for 3 h at 4°C. After washing five times with binding buffer, the protein-bead complex was boiled in SDS (sodium dodecyl sulfate) loading buffer and detected with an anti-GST antibody (EM80701, Hua An Biotechnology Co., Ltd, Hangzhou, China). 5% input was loaded as the control.

Isothermal titration calorimetry (ITC) and bo-layer interferometry (BLI) binding assays

ITC binding experiments were performed on a Microcal PEAQ-ITC instrument with a 19-injection setting. The running parameters were set to: temperature at 25°C, reference power at 5 μcal/s, stir speed at 0.75 rcf/s and the duration/spacing time of 4/150 s. The synthesized peptides were lyophilized and dissolved in the same buffer as MBP-tagged BP1 proteins with 100 mM NaCl, 20 mM HEPES, pH 7.5 and 3 mM β-mercaptoethanol. All the raw ITC data were processed using the Origin 7.0 program.

BLI experiments were carried out using a FortéBio Octet RED 96 system (Pall-fortébio Corporation). The biotinylated histone peptides were loaded onto streptavidin sensors (SA, #18–5019, Pall-fortébio Corporation) in 250 μl of SD buffer (0.1% BSA, 0.05% Tween 20, 10 mM PBS, pH 7.4) for equilibrium for 300 s. The associations of peptide with BP1-6 × His were tested by soaking the peptide-loaded sensors in the wells containing BP1-6 × His at different concentrations for 100 s. The dissociations of peptide from protein were tested by depriving sensors from the wells for 150 s. When the process of association and dissociation for one concentration were finished, 300 s of equilibration was performed to prepare for the next concentration. Finally, the results were calculated by FortéBio data analysis 10.0 software.

Chromatin immunoprecipitation (ChIP) and ChIP-seq analysis

ChIP of wild type PH-1 and Δ*BP1*-C assays was carried out with fresh mycelia grown in yeast extract peptone dextrose (YEPD) medium for 24 h and performed as previously described (23,30) using anti-H3K27me3 (39155, Active Motif) and anti-GFP (ab290, Abcam, Cambridge, UK) antibodies. Briefly, approximately two grams of mycelia were cross-linked with 1% formaldehyde for 20 min at room temperature and then stopped with 125 mM glycine. Samples were ground with liquid nitrogen and re-suspended in lysis buffer (250 mM, HEPES pH 7.5, 150 mM NaCl, 1 mM EDTA, 1% Triton, 0.1% deoxyCholate, 10 mM DTT) and protease inhibitor (Sangon Co., Shanghai, China). After centrifugation, the supernatant was diluted with 10 × ChIP dilution buffer (1.1% Triton X-100, 1.2 mM EDTA, 16.7 mM Tris−HCl, pH 8, 167 mM NaCl, 0.4 mM PMSF and protease inhibitor) before shearing the chromatin by sonication. The obtained chromatin was sonicated into DNA fragments between 200 and 500 bp using Diagenode Bioruptor (high setting, 18 cycles, every cycle with 30 s 'on' and 30 s 'off'). Samples were pre-washed with 20 μl of protein A agarose (sc-2001, Santa Cruz, CA, USA) for 1 h at 4°C. Then, the supernatant was incubated with 5 μl anti-GFP antibody (ab290, Abcam, Cambridge, UK) or anti H3K27me3 antibody (39155, Active Motif) overnight at 4°C, and then added into 20 μl of protein A agarose for 1.5 h at 4°C. The beads were washed in an orderly manner with low salt buffer (150 mM NaCl, 0.1% SDS, 1% Triton X-100, 2 mM EDTA, 20 mM Tris−HCl, pH 8), high salt buffer (500 mM NaCl, 0.1% SDS, 1% Triton X-100, 2 mM EDTA, 20 mM Tris−HCl, pH 8), LiCl buffer (0.25 M LiCl, 1% NP-40, 1% sodium deoxycholate, 1 mM EDTA, 10 mM Tris−HCl, pH 8), and TE buffer (10 mM Tris−HCl pH 8, 1 mM EDTA). The DNA-protein complex was reverse cross-linked and, DNA was recovered with phenol-chloroform extraction. The recovered DNA was used as a template for followed ChIP-seq and ChIP-qPCR. Three biological repeats were performed.

For the ChIP-seq assay, purified DNA was used for library construction with the NEBNext Ultra II DNA Library Prep Kit for Illumina (NEB, E7645L). Subsequently, high- throughput sequencing was carried out using an Illumina Hiseq-PE150 by Novogene Corporation (Beijing, China). The sequencing reads were mapped to the *F. graminearum* reference genome (FungiDB-44_*F. graminearum* PH-1_Genome) using BWA (Burrows Wheeler Aligner v 0.7.12) software. The genome ChIP-seq profiles were generated using MACS 2.1.0 with only uniquely mapped reads (Supplementary Table S2). Peaks were called at *P* values ≤0.005 with input DNA as a control. To validate the ChIP-seq results, ChIP-qPCR assay was performed. The mRNA levels of the tested genes were relative to the internal reference gene *ACTIN* using quantitative real-time PCR.

RNA-seq analysis

Total RNA was isolated from three independent biological replicates from the wild type PH-1, the deletion mutant Δ*Kmt6*, and Δ*BP1*. DNA-free total RNA was generated by the NEBNext® Ultra™ RNA Library Prep Kit for Illumina® following the manufacturer's recommendations and index codes were added to attribute sequences to each sample. Library quality was assessed on an Agilent Bioanalyzer 2100 system. Clustering of the index-coded samples was performed on a cBot Cluster Generation System using TruSeq PE Cluster Kit v3-cBot-HS (Illumina) according to the manufacturer's instructions. After cluster generation, the library preparations were sequenced on an Illumina Novaseq platform and 150 bp paired-end reads were generated. The sequencing reads were mapped to the *F. graminearum* genome (FungiDB-44_*F. graminearum* PH-1_Genome) using HISAT 2 v2.0.5 software. Feature Counts v1.5.0-p3 was used to count the reads mapped to each gene. Differential gene expression was determined by DESeq2 v1.16.1 (*P* value ≤ 0.05; fold change ≥ 2.0). We used cluster Profiler R package to test the statistical enrichment of differentially expressed genes in KEGG pathways.

Electrophoretic mobility shift assay (EMSA)

The Cy3-labeled DNA fragments were incubated with increasing amounts of purified MBP-BP1, $BP1^{\Delta BAH}$ or $BP1^{\Delta PHD}$ protein in 1× binding buffer (10 mM Tris pH 7.5, 100 mM NaCl, 0.1 mM DTT and 5% glycerol) for 30 min on ice. After the reaction, 2.5 μl of 10× loading buffer (10 mM Tris pH 7.5, 1 mM DTT, 50% vol/vol glycerol, 0.001% wt/vol bromophenol blue, 0.001% wt/vol xylene cyanol FF) was added to stop the reaction and analyzed by 5% native PAGE. Gel electrophoresis was performed with cold 0.5× Tris/borate/EDTA running buffer at 100 V for 60 min on the ice. Cy3-labeled DNA fragments in the gel were analyzed with Typhoon 5 and quantified by using ImageQuant (Amersham, GE Helthcare).

MNase-qPCR

The MNase (micrococcal nuclease)-qPCR assay was used to measure nucleosome occupancy. Fresh mycelia were harvested in liquid nitrogen and ground to a fine powder using a precooled mortar and pestle, and then nuclei were isolated as previously described (31). The isolated DNA (70–80 ng) was digested with 0.5 μl of micrococcal nuclease (final concentration 0.01–0.02 units/μl, Takara) for 8 min in digestion buffer at 37°C. Mononucleosomes were then excised from 1.5% agarose gels and purified using a gel purification kit. The purified DNA was quantified using a NanoDrop ND-1000 spectrophotometer. The nucleosome occupancy was calculated with the $2^{-\Delta\Delta}$Ct method using undigested genomic DNA followed by normalization over that of Actin 100+ loci for each sample. The tiled primer sets used for real-time PCR are listed in Supplementary Table S1. Three independent experiments were performed for the MNase-qPCR assay.

Pathogenicity assays

The conidia of each strain formed in CMC medium were collected and suspended in sterile distilled water to a final concentration of 10^5 conidia ml^{-1}. A 10 μl suspension of fresh conidia of each strain was injected into a floret in the

central section spikelet of a single flowering wheat head of the susceptible cultivar Zimai22. At 15 days after inoculation, the infected spikelets in each inoculated wheat head were recorded. For wheat leaf infection, fresh mycelial plugs of each strain were inoculated in the middle of the leaves and incubated in a growth chamber at 25°C. Images were taken 6 days after inoculation. Corn silk infection assays were carried out essentially as described above for wheat leaf infection. The images were taken at 5 days post-inoculation. There were 15 replicates for each strain in each experiment, and three biological replicates were conducted.

RESULTS

Identification of PRC2 components in *F. graminearum*

Candidate core PRC2 components in *F. graminearum*, Kmt6 (FGSG_15795), Eed (FGSG_15909) and Suz12 (FGSG_04321), were previously identified with respective *Drosophila* homologs through BLASTp (32). They contain representative domains as their corresponding homologs (Figure 1A). To determine whether these three proteins indeed interact with each other and form a complex, we first fused each candidate component to GFP and observed their subcellular localization in *F. graminearum*. As shown in Figure 1B, all three subunits were primarily co-localized to nuclei stained with DAPI in the mycelia, suggesting that these components may form a complex in the nucleus, similar to PRC2 in other species. Then, we performed an ACMS assay using individual proteins fused with 3× Flag or GFP as baits to test whether these subunits interact with each other *in vivo*. The results showed that each bait protein could capture the other two candidate components (Figure 1C, Supplementary Table S3). Co-IP assays with strains expressing Kmt6-Flag and Eed-GFP, Kmt6-Flag and Suz12-GFP or Suz12-Flag and Eed-GFP confirmed these interactions *in vivo* (Supplementary Figure S1A). Furthermore, Y2H assays indicated that Kmt6 physically interacted with Eed and Suz12 (Figure 1D, Supplementary Figure S1B). Together, these results suggest that Kmt6-Suz12-Eed forms a complex in this fungus.

To determine whether this complex functions similar to PRC2 to catalyze H3K27 methylation in this fungus, single gene deletion mutants Δ*Kmt6*, Δ*Eed* and Δ*Suz12* displayed similar colony morphology with dramatically reduced growth on PDA and were nonpathogenic as compared with wild-type PH-1 (Figure 1E, Supplementary Figure S2). Importantly, disruption of each of these gene completely abolished H3K27me3 modification but did not affect H3K4 or H3K36 trimethylation (Figure 1F). The defect in hyphal growth and aberrant H3K27me3 levels in these mutants were completely restored in the corresponding gene-complementation strains (−C) under the tested conditions (Figure 1E-F, Supplementary Figure S2).

Notably, a Nurf55 homolog also exists in the genome of *F. graminearum* at the FGSG_16720 locus (Supplementary Figure S3A). However, the deletion mutant of FGSG_16720 exhibited different phenotypes, as compared to those of the Δ*Kmt6*, Δ*Eed* and Δ*Suz12* mutants, and the H3K27 methylation level was not significantly affected in the FGSG_16720-deletion mutant (Supplementary Figure S3B, C). Thus, the Nuf55 homolog might not be a component of the PRC2 in this fungus. Taken together, the data show that Kmt6 mediates the interaction between Suz12 and Eed, that these proteins form a PRC2 complex to catalyze H3K27me3 in *F. graminearum*.

BP1 protein interacts with Suz12

To identify factors associated with PRC2 for H3K27me3-mediated gene silencing, we analyzed putative domains in all the proteins captured by PRC2 components in the ACMS assay. One protein (FGSG_11913) drew our attention because it was captured by all three core PRC2 components when they were used as baits, and confirmed by Co-IP (Figure 1C, Supplementary Figure S4A and B, Table S3). FGSG_11913 contains a BAH domain followed by a plant homeodomain (PHD) (Figure 2A). Since both BAH and PHD were previously reported to be associated with PRC2 readers in plants and animals (19–24), we hypothesized that the BAH-PHD protein encoded by the FGSG_11913 locus may be a potential accessory of PRC2, and is thus hereafter called BP1 (BAH-PHD protein 1). All three core PRC2 components could be captured when BP1 was used as a bait in the ACMS assay (Supplementary Table S3). To verify whether BP1 indeed interacts with PRC2, Y2H assays were conducted, and the results showed that BP1 directly interacted with Suz12 but not Kmt6 or Eed (Figure 2B, Supplementary Figure S4C). The interaction between BP1 and Suz12 was further confirmed by fluorescence co-localization and Co-IP. Both fluorescence fused proteins were localized to nuclei in the mycelia of strains expressing Suz12-GFP and BP1-mCherry (Figure 2C, upper panel). The interactions between BP1-Flag and Suz12-GFP were detectable by Co-IP in two directions (Figure 2D). Furthermore, the deletion mutant Δ*BP1* displayed similar growth phenotypes and virulence as the mutants of PRC2 core components (Figures 1E and 2E, Supplementary Figure S2). Thus, these results suggest that BP1 is associated with PRC2 by interacting with Suz12 (Figure 2F).

To determine whether the BAH domain and the PHD finger are necessary for the interaction between BP1 and Suz12, truncated proteins $BP1^{\Delta BAH}$ and $BP1^{\Delta PHD}$, lacking either the BAH domain and PHD finger, respectively, were generated. We found that neither truncated protein interacted with Suz12 in Y2H assays (Figure 2B, Supplementary Figure S4C). Although the mCherry labeled $BP1^{\Delta BAH}$ and $BP1^{\Delta PHD}$ still co-localized with Suz12-GFP in nuclei (Figure 2C), the growth-defective phenotype of Δ*BP1* was not rescued by either $BP1^{\Delta BAH}$ or $BP1^{\Delta PHD}$ (Figure 2E). Therefore, both the BAH domain and PHD finger in BP1 are essential for the BP1 interaction with PRC2 and for functional BP1 activity. Surprisingly, the total level of H3K27me3 in the Δ*BP1* strain was comparable to that in the wild type PH-1 (Supplementary Figure S4D), in contrast to the mutants of core components of PCR2 (Figure 1F), suggesting that BP1 might act as a downstream effector of PRC2.

In the genome of *F. graminearum*, 27 putative proteins contain either the BAH or PHD domain, and two contain both domains (Supplementary Table S4). To test whether these other BAH domain- or PHD finger-containing proteins are involved in PRC2, in addition to BP1, we first

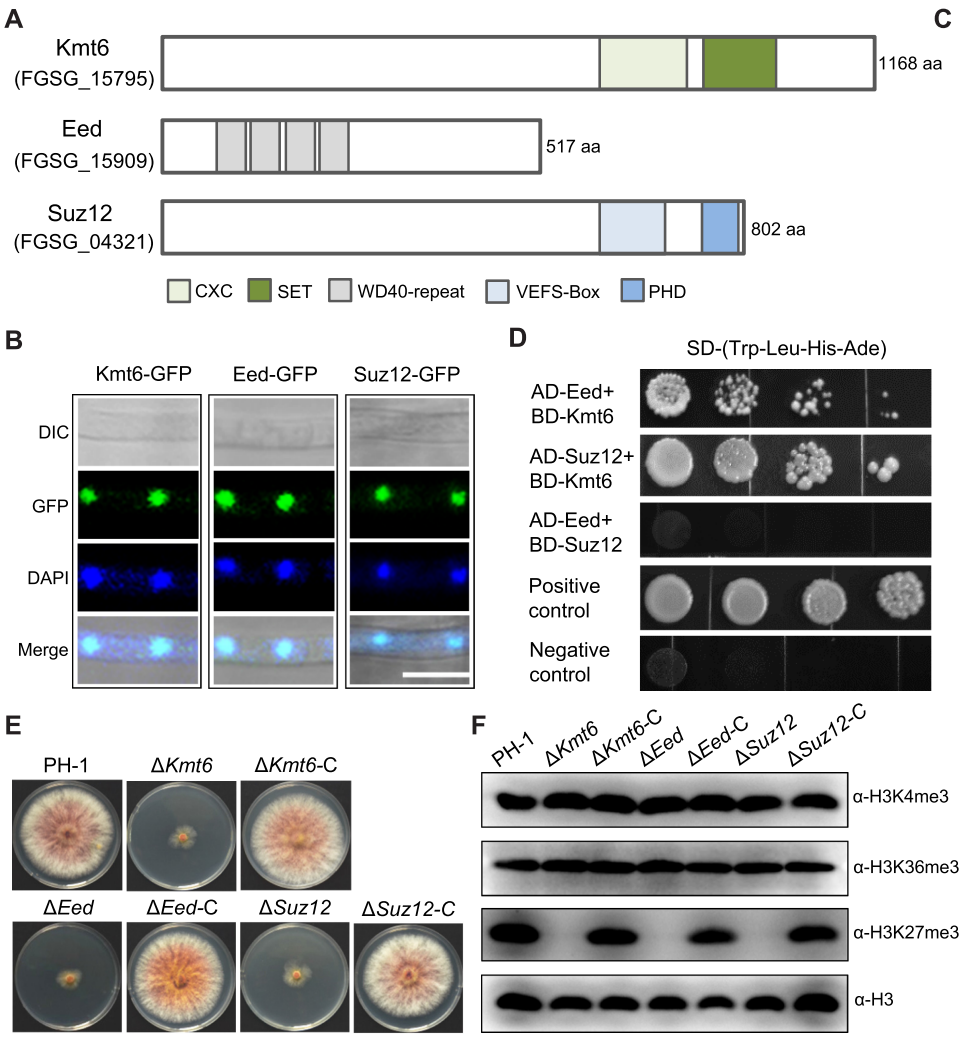

C

Kmt6-3xFlag			
Interactors	Repeat	Unique Peptides	Score Mascot
Suz12	1	24	861
	2	13	657
	3	18	822
Eed	1	8	279
	2	5	171
	3	5	149
FGSG_11913	1	25	2136
	2	23	2161
	3	23	1893

Eed-GFP			
Interactors	Repeat	Unique Peptides	Score Mascot
Suz12	1	30	1415
	2	29	1419
	3	14	627
Kmt6	1	35	1812
	2	38	1290
	3	22	854
FGSG_11913	1	27	3425
	2	29	2786
	3	22	1319

Suz12-GFP			
Interactors	Repeat	Unique Peptides	Score Mascot
Kmt6	1	50	3020
	2	25	970
	3	51	2737
Eed	1	20	1629
	2	10	608
	3	22	1507
FGSG_11913	1	29	3864
	2	20	1341
	3	29	3992

Figure 1. Kmt6, Eed, and Suz12 are core PRC2 components in *F. graminearum*. (**A**) Domain architecture of putative core PRC2 components. (**B**) Kmt6, Eed and Suz12 localize to the nucleus. Proteins were fused with GFP and transformed into the wild type, and visualized by confocal microscopy. DAPI staining was used to indicate the nucleus. DIC, differential interference contrast. Scale bar: 10 μm. (**C**) Summary of the main interactors of Kmt6, Suz12 and Eed as identified by affinity capture-mass spectrometry (AC-MS) analysis. Fungal strains stably expressing FLAG-tagged Kmt6, GFP-tagged Eed or Suz12 were individually subjected to FLAG or GFP affinity purification followed by MS. (**D**) Kmt6 interacts with Eed and Suz12 in yeast cells. The full-length protein was fused with the GAL4-AD or BD domain, as indicated. Serial concentrations of yeast cells were assayed for growth on selected medium without tryptophan, leucine, histidine and adenine. pGBKT7-53 + pGADT7 and pGBKT7-Lam with pGADT7 were used as the positive and negative control, respectively. (**E**) Mutants of core PRC2 components showing reduced mycelial growth on potato dextrose agar plates. The wild type PH-1, deletion mutants and corresponding complementation strains (−C) were inoculated on potato dextrose agar plates and incubated at 25°C for 3 days. (**F**) Mutants of core PRC2 components abolished H3K27me3 but not H3K4me3 or H3K36me3 marks. Total proteins in corresponding strains were extracted, and specific proteins were detected by immunoblotting using the indicated antibodies. The protein samples were also detected with an anti-H3 antibody used as a loading control.

attempted to knock out these individual genes and examine the growth rates of mutants. Ideally, if a protein is important for PRC2-mediated gene silencing, the disruption mutant of this protein would display growth defect phenotypes on PDA similar to those of the mutants of the core PCR2 components. Using homologous recombination, we successfully disrupted 26 of 29 genes. Repeated efforts to delete the remaining 3 genes failed, likely because the mutations may have been lethal. Among the 26 mutants, eight mutants exhibited visually reduced mycelial growth (Supplementary Figure S5A). Next, we performed a Y2H assay to determine whether the proteins encoded by the eight growth-associated genes and three lethal genes were able to physically interact with PRC2 core components. As shown in Supplementary Figure S5B, none of the 11 tested proteins interacted with Kmt6, Suz12 or Eed. Therefore, we infer that BP1 is the sole BAH-PHD protein interacting with the PRC2 complex in this fungus.

BP1 is a reader of methylated H3K27

Histone readers can recognize and directly bind post-translationally modified histones through specific domains, such as the BAH domain and PHD finger (18,19,33). Given

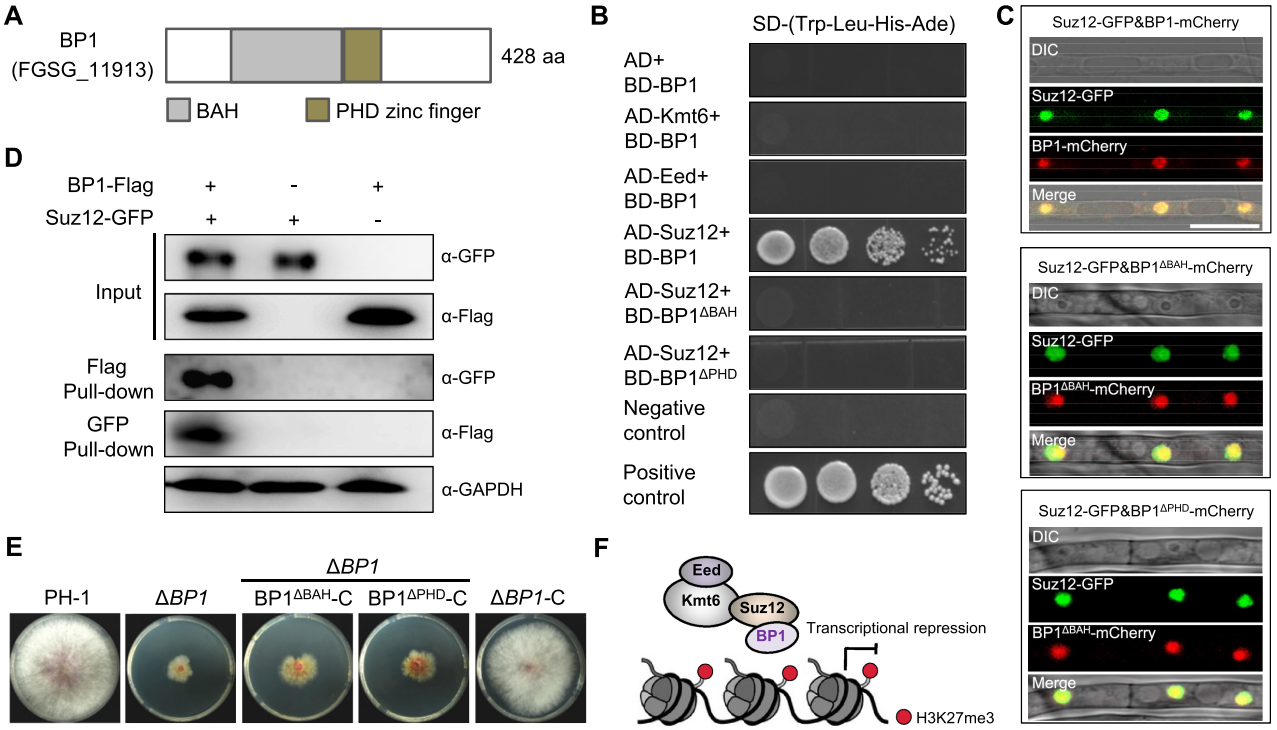

Figure 2. BP1 associates with PRC2 *via* Suz12. (**A**) Schematic representation of BP1 and its domains. (**B**) BP1 interacts with Suz12 depending on both the BAH domain and PHD finger in yeast cells. The full-length protein or truncated BP1 variants BP1$^{\Delta BAH}$ and BP1$^{\Delta PHD}$ were fused with the GAL4-AD or BD domain, as indicated. Serial concentrations of yeast cells were assayed for growth on selected medium without tryptophan, leucine, histidine and adenine. (**C**) BP1-mCherry co-localizes with Suz12-GFP in the nucleus via either the BAH or PHD finger. Vegetative hyphae of dual-labelled strains were observed under a confocal microscope after incubation in PDB medium for 24 h. DIC, differential interference contrast. Bar = 10 μm. (**D**) Coimmunoprecipitation of BP1 and Suz12. BP1-Flag was immunoprecipitated by anti-GFP from the total protein lysates of a dual-labelled strain expressing Suz12-GFP and BP1-Flag, and vice versa. (**E**) BAH and PHD finger domains are essential for BP1 function in vegetative growth. The wild type PH-1, ΔBP1 and corresponding complementation strains (-C) were inoculated on potato dextrose agar plates and incubated at 25°C for 3 days. (**F**) Diagram of the inferred BP1-PRC2 interaction pattern.

that BP1 is a BAH-PHD protein and interacts with components in the PRC2, we tested the binding capability of BP1 to methylated H3K27 peptides. We first performed a histone peptide pull-down assay using purified GST-BP1 protein. The results indicated that GST-BP1 could be pulled down by H3K27me1, H3K27me2 and H3K27me3 peptides in a sequentially increasing manner but could not pull down un-methylated H3K27 or H3K36me3 peptides (Figure 3A). The H3K4me3 peptides were also able to pull down GST-BP1 but to a much lesser extent than methylated H3K27 peptides (Figure 3A). The methylated H3K27 peptide-binding activity was confirmed by ITC binding analysis (Figure 3B). Moreover, BLI results also showed that BP1 could bind methylated H3K27 peptides (Supplementary Figure S6). Consistent with the histone pull-down results, BP1 showed a binding preference for H3K27 with a higher methylation level (Figure 3B). Furthermore, we found that the truncated protein BP1$^{\Delta BAH}$, but not BP1$^{\Delta PHD}$, showed abolished binding activity to H3K27me3 peptides in histone peptide pull-down assays, suggesting that the BAH domain of BP1 was critical for its binding activity with methylated H3K27 peptides (Figure 3C). This evidence fully demonstrates that BP1 is a H3K27-methylation reader in *F. graminearum*.

BP1 is distributed in a set of genomic regions marked by H3K27me3

Considering that BP1 is associated with PRC2 and directly binds the methylated H3K27 peptides, we sought to determine whether BP1 genomic targets coincided with H3K27me3 throughout the genome using ChIP-seq. The Δ*BP1* mutant was in a locus complemented with a BP1-GFP fusion cassette under its native promoter. The complemented strain Δ*BP1*::P_{BP1} BP1-GFP was subjected to ChIP-seq with an anti-GFP antibody. H3K27 trimethylated genomic regions were immunoprecipitated with an anti-H3K27me3 antibody. In agreement with the findings of a previous study (32), H3K27me3 was found in all four chromosomes, predominantly in subtelomeric regions in *F. graminearum*. As predicted, the results of BP1-GFP ChIP-seq indicated that BP1 exhibited a similar distribution as H3K27me3 on the chromosomes in the wild-type fungus (Figure 4A). Both BP1 and H3K27me3 were enriched in gene bodies extending from the transcription start site (TSS) to regions near the transcription termination site (TTS) (Figure 4B). We identified a total of 4071 significant BP1 peaks (P value $\leq$ 0.005), corresponding to 2363 genes. To overlap the BP1-associated genes with H3K27me3-marked genes, we performed Venn diagram

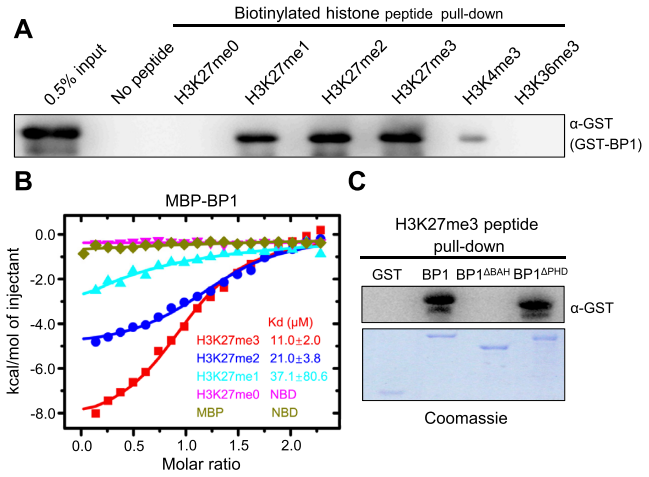

Figure 3. BP1 binds methylated H3K27 histone peptides. (**A**) Immunoblots showing the pull-down results for GST-BP1 using different biotinylated histone peptides. Precipitation was analyzed with an anti-GST antibody. The 0.5% input served as the positive control. (**B**) ITC binding curves showing the MBP-BP1 binding preference for histone H3 with different K27 methylation levels. The MBP tag was used as a control. NDB, no detectable binding. (**C**) Immunoblots showing the pull-down results for GST-labeled BP1 and truncated proteins using H3K27me3 peptides. GST served as a control. The precipitation of biotinylated H3K27me3 was analyzed with an anti-GST antibody. The amount of GST proteins were controlled by Coomassie staining.

analysis and found that 44% (1045 of 2363) of BP1-bound genes overlapped with H3K27me3 marked genes (Figure 4C). A KEGG analysis revealed significant enrichment of overlapping genes involved in several important biological processes, such as cyanoamino acid metabolism, starch and sucrose metabolism and secondary metabolic biosynthesis (Figure 4D). We selected five loci co-occupied by BP1 and H3K27me3 in different chromosomes and validated the enrichment of BP1 and H3K27me3 at the gene body regions of these five loci using ChIP and qPCR (Figure 4E and F). Altogether, these results illustrate that BP1 co-occupies a large number of genomic regions marked with H3K27me3 *in vivo*. Notably, H3K27me3 enrichment was absent in some regions of BP1-GFP occupied genes and vice versa (Supplementary Figure S7).

BP1 depletion relieves the gene transcription repressed by Kmt6

It was previously shown that thousands of genes were derepressed following disruption of PRC2 in fungi (32,34). Given that BP1 co-occupies a large number of genomic regions marked with H3K27me3, it is reasonable to deduce that BP1 might be involved in H3K27me3-mediated gene repression. To test this hypothesis, we performed RNA-seq experiments with mRNA extracted from the mycelia of wild-type, Δ*Kmt6* and Δ*BP1* mutants grown in YEPD to determine their transcriptional profiles. Consistent with the findings of a previous study (32), we found more up-regulated genes than down-regulated genes in the Δ*Kmt6*, with 4224 *versus* 1040 genes, respectively (P value < 0.05, fold change > 2) (Figure 5A). Similar to the transcriptional patterns of Δ*Kmt6*, 4805 genes were dysregulated in the Δ*BP1* strain, with 3896 up-regulated and 909 down-regulated genes (Figure 5B, Supplementary Data 1). A Venn diagram showed a significant overlap in up-regulated genes between the Δ*BP1* and Δ*Kmt6* strains (3651 genes, representing ∼94% of the up-regulated genes in Δ*BP1*) (Figure 5C, Supplementary Data 2). Among these genes, 715 genes (20% of the overlapping up-regulated genes) were co-occupied by H3K27me3 and BP1 (Figure 5D), indicating that these genes were repressed directly by BP1 and H3K27me3.

A KEGG analysis indicated that genes co-repressed by BP1 and Kmt6 are involved in both primary and secondary metabolisms, including metabolism of amino acids and carbon, as well as the biosynthesis of secondary metabolites (Figure 5E).In addition, Kmt6 has been identified as a repressor of secondary metabolism in *F. graminearum* (32), suggesting that BP1 may also negatively regulate secondary metabolism. To visualize the effects of BP1 on the regulation of secondary metabolite (SM) genes (35), we generated heat-maps of transcriptional changes in the Δ*BP1* and Δ*Kmt6* strains and compared to the wild type, including genes encoding polyketide synthases (PKS), nonribosomal peptide synthases and cytochrome P450 enzymes in *F. graminearum*. As shown in Figure 5F, 74% of the tested genes (80 of 109 genes) were significantly up-regulated more than 2-fold compared to those in the wild type, showing almost the same expression patterns as those of the Δ*Kmt6* strain. RT-qPCR of selected SM genes in the mutants and wild type confirmed the RNA-seq results (Figure 5G) and further suggested that BP1 represses the biosynthesis of secondary metabolites. Taken together, these results suggest that BP1 facilitates gene repression, and regulates an overlapping set of PRC2 target genes, especially secondary metabolic genes.

BP1 has DNA-binding activity that depends on its PHD finger

Increasing evidence suggests that histone reader domains have nucleic acid-binding activity (36). Considering that BP1 contains both BAH and PHD finger domains, we thus determined potential DNA-binding activity of BP1. The top 500 peak sequences occupied by BP1-GFP in the ChIP-seq data were used to search for potential DNA binding motifs of BP1 by MEME SUITE online software (37). The top 10 output motifs showed diversity without clear sequence specificity (Supplementary Figure S8A). Subsequently, four different motifs were randomly selected and further subjected to testing for DNA-binding activity of BP1. As shown in Figure 6A, increasing the amount of the purified fused protein MBP-BP1 strongly retarded the electrophoretic mobility of all four tested DNAs, in contrast to the results of MBP alone in the EMSA. The DNA-binding activity was further validated by ITC assay (Supplementary Figure S8B). These results suggest that BP1 can bind DNA but might not show sequence specificity. Thus, we selected five random DNA fragments and determined whether they could bind to BP1 by performing an EMSA. As shown in Supplementary Figure S9, BP1 could bind all tested DNA fragments. Collectively, our results reveal

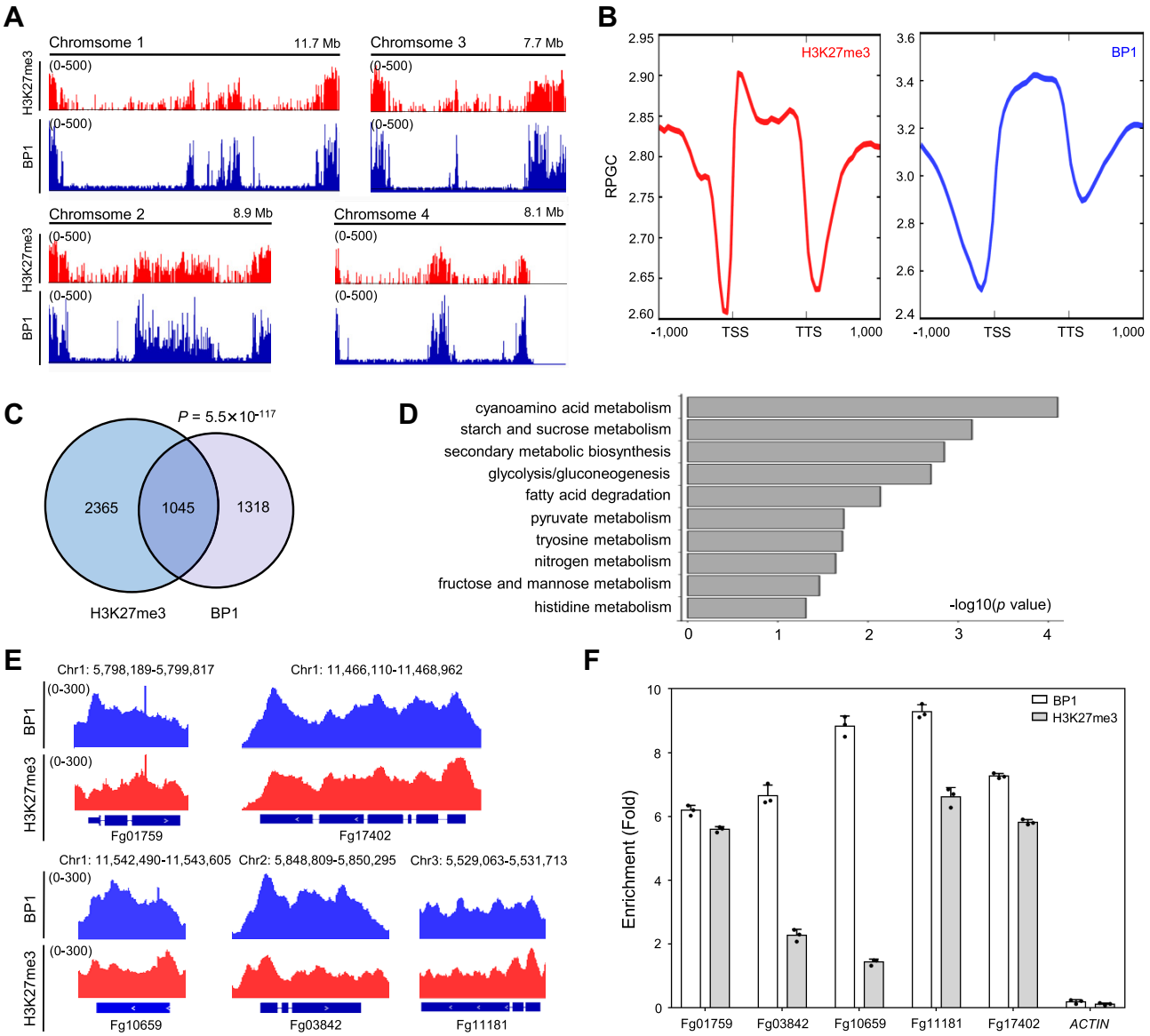

Figure 4. BP1 localizes to H3K27me3 genome-wide. (**A**) ChIP-seq signals within four chromosomes of *F. graminearum* as detected with an anti-H3K27me3 antibody (red) and anti-GFP antibody targeted to BP1-GFP (blue). The Y-axis represents the RPM, reads per million (the read coverage was normalized by the total number of mapped reads). The track scales of BP1 and H3K27me3 ranged from 0 to 500. (**B**) Metagene plots of H3K27me3 and BP1 distribution at target transcription units and flanking intergenic regions. TSS, transcription start site and TTS, transcription termination site. The y-axis scales represent reads per genomic content (1 × normalization) (RPGC). (**C**) Venn diagram showing statistically significant overlapping between the genes targeted by BP1-GFP and those occupied by H3K27me3. *P* values (Fisher's exact test) for overlapping between gene sets are indicated. (**D**) KEGG analysis results of BP1 and H3K27me3 of overlapping target genes. (**E**) Genome-browser view of normalized BP1-GFP (blue) and H3K27me3 (red) ChIP-seq peaks at selected targeted genes. The y-axis represents the RPM. The track scale of BP1 ranged from 0 to 300. (**F**) ChIP-qPCR assay showing that BP1-GFP and H3K27me3 were significantly enriched at the gene body regions of selected targeted genes. ChIP and input-DNA samples were quantified by quantitative PCR. *ACTIN* served as the control locus. Relative enrichment of BP1 and H3K27me3 at the indicated loci was normalized to input. The data represent the mean ± standard deviation (s.d.) ($n = 3$ biological repeats).

that BP1 has strong DNA-binding ability with no sequence specificity.

Next, the secondary metabolic gene Fg00012 encoding a cytochrome P450 oxidoreductase was selected as a target gene to further investigate which domain is critical for the DNA-binding activity of BP1. The gene was occupied and repressed by both BP1 and H3K27me3 in the ChIP-seq analysis (Figure 6B, upper panel). ChIP-qPCR confirmed the co-occupancy and revealed that BP1 and H3K27me3 were mainly enriched at the gene body region (Figure 6B, middle and bottom panels). Then, a DNA fragment in the Fg00012 gene body region was used as the DNA substrate (5′-GTAGTTGACAAAGGTGAACACAGC-3′) in an EMSA assay to determine its affinity with full-length MBP-BP1 and truncated proteins, MBP-BP1$^{\Delta BAH}$ and MBP-BP1$^{\Delta PHD}$. EMSA results showed that MBP-BP1 and MBP-BP1$^{\Delta BAH}$ strongly retarded the electrophoretic mobility of the tested DNA fragment, whereas MBP-BP1$^{\Delta PHD}$

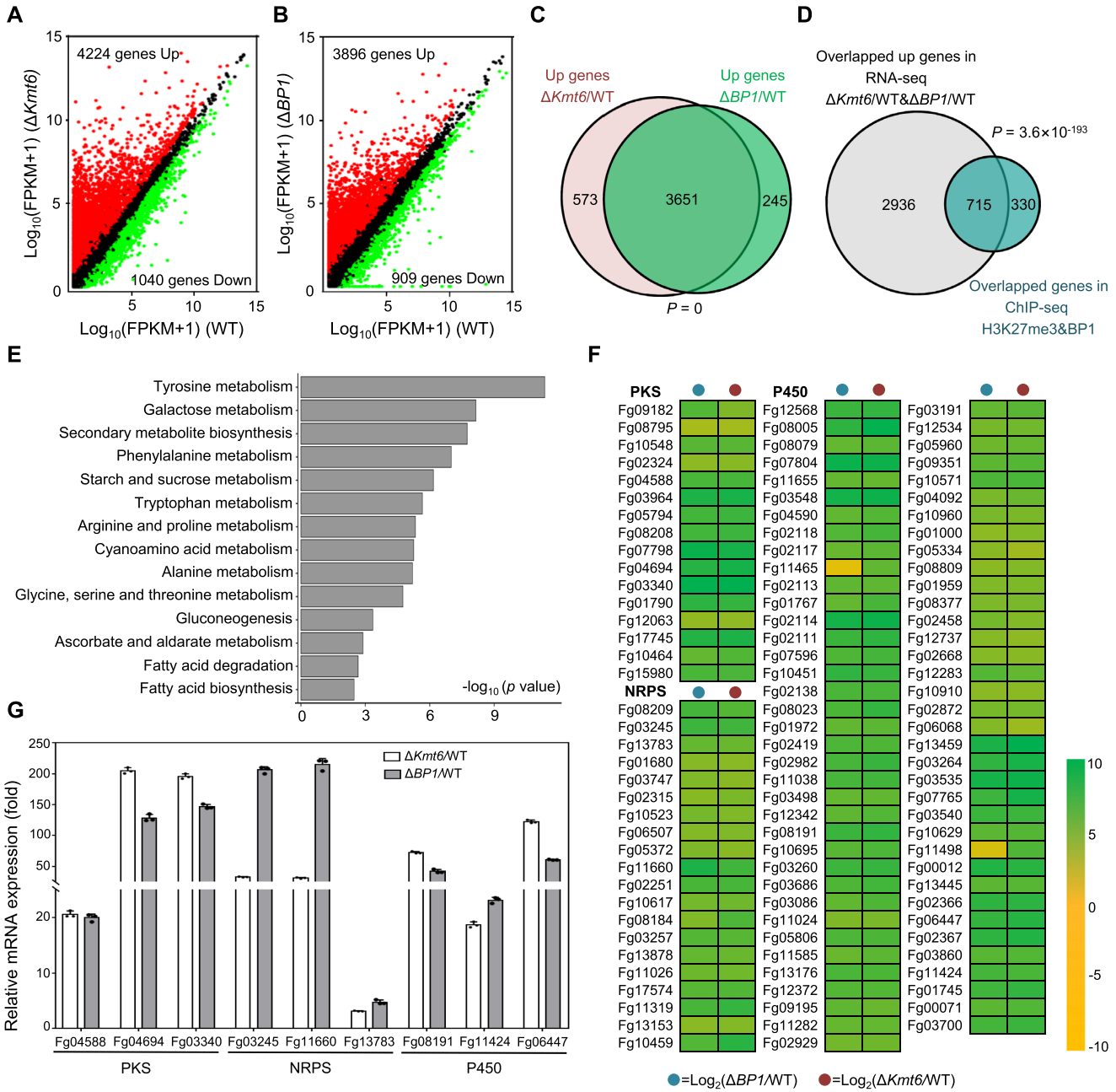

Figure 5. BP1 represses an overlapping set of H3K27 trimethylated genes. (**A**, **B**) Scatter plot showing changes in gene expression as detected by RNA-seq in Δ*Kmt6* and Δ*BP1* strains compared to the wild type PH-1, respectively. Up- and down-regulated genes are highlighted in red and green, respectively. Expressed genes with fold-change ≥2 and *P*-value ≤0.05 were regarded as significantly different. The remaining genes are shown in black. (**C**) Venn diagram analysis showing up-regulated genes in both Δ*Kmt6* and Δ*BP1* strains compared with those in PH-1. *P* values (Fisher's exact test) for overlapping between gene sets are indicated. (**D**) Venn diagrams showing statistically significant overlapping between up-regulated genes in the mutants and genes co-occupied by both BP1-GFP and H3K27me3. (**E**) KEGG analysis of overlapping and up-regulated genes after loss of Δ*Kmt6* and Δ*BP1*. (**F**) Heat-maps showing transcriptional changes of selected secondary metabolic biosynthetic genes in mutant strains compared to those in the wild type, including genes encoding polyketide synthase (PKS), non-ribosomal peptide synthase (NRPS) and cytochrome P450 enzymes in *F. graminearum*. (**G**) Expression levels of selected genes presented in the f panel were verified by RT-qPCR for the wild type PH-1, Δ*Kmt6* and Δ*BP1* strains. Actin served as a control. Each error bar represents the s.d. of a mean obtained from three independent experiments.

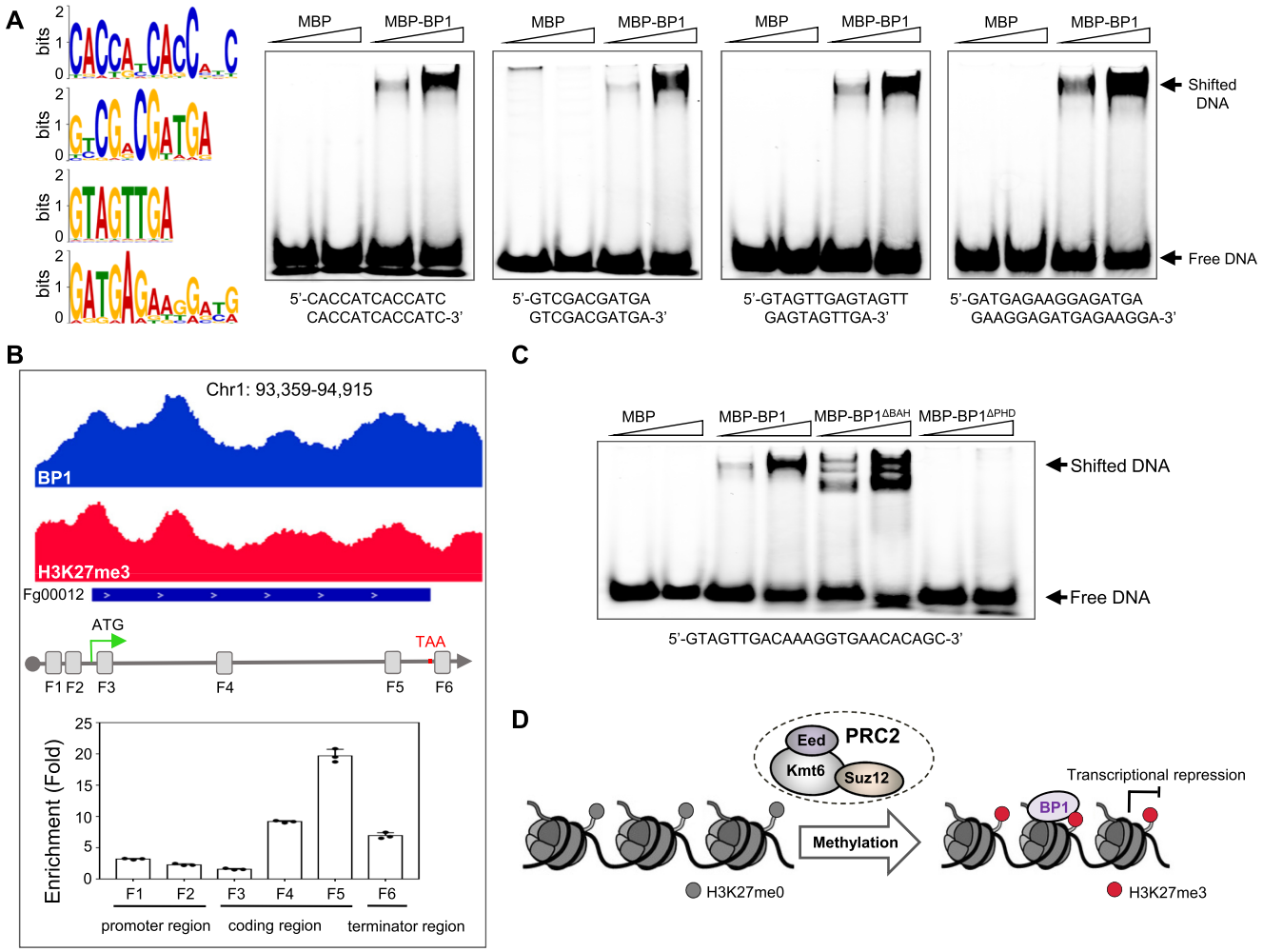

Figure 6. BP1 is able to bind DNA *via* its PHD finger. (**A**) Electrophoretic mobility shift assay (EMSA) assessing the DNA-binding activity of BP1. Four over-represented BP1-binding motifs and their representative DNA fragments were used as DNA substrates. The purified MBP tag was used as a control. (**B**) Genome browser view of normalized BP1 (blue) and H3K27me3 (red) ChIP-seq peaks at the Fg00012 genomic region. Chip-seq peaks showing the diagram of the loci assessed and regions amplified by ChIP-qPCR. ChIP-qPCR assays revealed that BP1 was significantly enriched in the Fg00012 coding region. ChIP and input DNA samples were quantified by quantitative PCR assays. Relative enrichment of BP1 at Fg00012 genomic region was normalized to input. F indicates the fragment amplified by PCR using the corresponding primers. (**C**) DNA-binding activity of MBP-BP1, MBP-BP1$^{\Delta BAH}$ and MBP-BP1$^{\Delta PHD}$ to the specified DNA fragment as determined by EMSA. The MBP tag was used as a control. (**D**) Schematic diagram of BP1-PRC2 mediated gene transcriptional repression.

totally abolished the capability to retard DNA mobility (Figure 6C). Together, these findings suggest that BP1 can directly bind DNA largely depended on its PHD domain. Considering the evidence to this point in our study, we proposed the following mechanism for PRC2-BP1 mediated gene transcriptional repression: PRC2 trimethylates H3K27 at the targeted region of chromosomes, and then, H3K27me3 is read by the downstream reader BP1, which might subsequently result in nucleosome retention through the DNA-binding activity of BP1 (Figure 6D).

BP1 orthologs are mainly distributed in fungi

To determine whether BP1 orthologs exist in other organisms, we searched BP1 orthologs from a BLASTp search against the NCBI non-redundant protein sequence database using BP1 as the query sequence, followed by BAH domain and PHD finger architectural analysis. A total of 633 orthologs were retrieved, representing 633 fungal and plant species, as well as other eukaryotes mainly in the fungal kingdom (Figure 7A, Supplementary Data 3). Notably, the BP1 ortholog in *Neurospora crassa*, EPR-1, was recently identified as an effector of Polycomb repression, indicating that the ortholog BP1 may be functionally conserved in fungal PRC2 mediated gene silencing (13). BP1 shows 37.7% amino acid sequence identity with EPR-1, especially in the BAH domain and PHD finger (Supplementary Figure S10A, Figure 7B-C). To test whether BP1 and EPR-1 are functionally interchangeable, a heterologous complementation experiment was conducted. EPR-1 was integrated into a Δ*BP1* strain to the native locus and expressed using the BP1 promoter. The resulting transformants were identified by PCR and immunoblotting (Supplementary Figure S10B, C). As expected, EPR-1 was able to partly rescue the growth defect and attenuated virulence in Δ*BP1* strain (Figure 7D-E). In addition, we com-

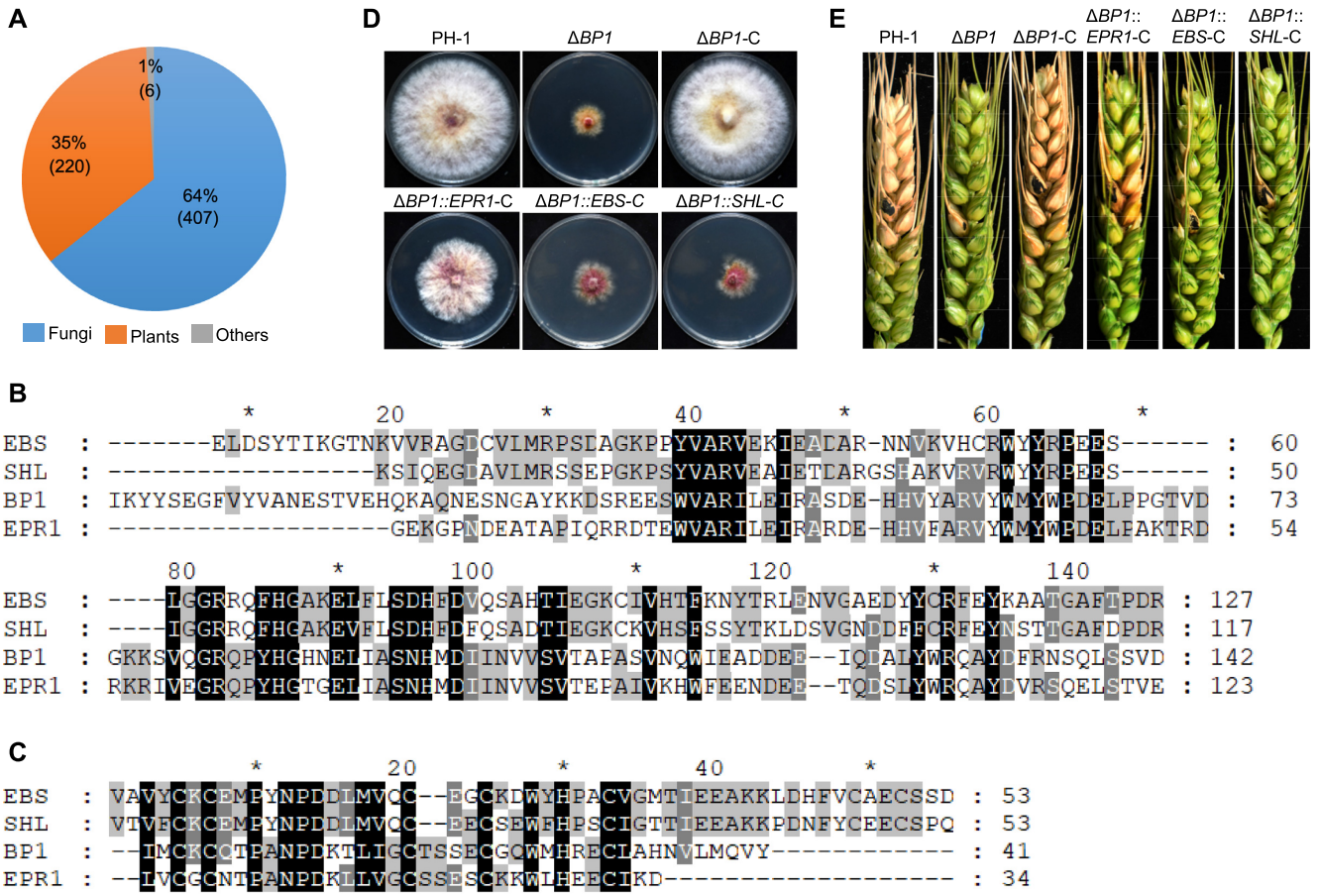

Figure 7. BP1 orthologs are widely distributed in eukaryotes. (**A**) Distribution of BP1 orthologs by kingdom. The number of orthologs in different kingdoms and the percentage of each in the total of the retrieved orthologs are shown. (**B**, **C**) Amino acid alignment of the BAH domain and PHD finger in BP1, the ortholog EPR1 in *Neurospora crassa* and EBS and SHL in *Arabidopsis thaliana*. The conserved residues are indicated below the alignments. (**D**) Colony morphology of the wild type PH-1, Δ*BP1*, Δ*BP1* complementation strains ΔBP1-C and ΔBP1 heterogenous complementation strains ΔBP1::*EPR1*-C, Δ*BP1*::*EBS*-C and Δ*BP1*::SHL-C grown on PDA medium for 3 days at 25°C. (**E**) Virulence of the wild type PH-1, Δ*BP1* and complementation strains on wheat heads. Disease symptom of the tested strains on wheat heads were recorded at 15 day post-inoculation.

plemented the Δ*BP1* using its orthologs from *Arabidopsis thaliana*, EBS and SHL, which contain a BAH domain and PHD finger and were identified as H3K27me3 readers in *A. thaliana*. As shown in Figure 7D, E, EBS and SHL failed to complement the defects in Δ*BP1*, which may have been due to the sequence variations in the BAH domain and PHD finger (Figure 7B, C). Meanwhile, EBS and SHL regulation of gene repression was previously shown to be largely dependent on Polycomb repressive complex 1 (PRC1) in *A. thaliana* (22). These results suggested that BP1 orthologs may be functionally conserved in fungi.

DISCUSSION

The polycomb protein complex-mediated transcriptional repression has been extensively studied in plants and animals. Various PRC1 and PRC2 complexes containing alternative components or accessory proteins have been identified (3,38). Recently, increasing evidence has indicated that PRC2 complex also exists in fungi (7). Although fungal PRC2 is considered to be relatively simple compared with its counterparts in higher eukaryotes, compositions of fungal PRC2 were previously shown to vary in different species (7). Genetic evidence and crystal structures revealed that homologs of animal Ezh2-Eed-Suz12 are core subunits in the ascomycetes *Neurospora crassa* and *Chaetomium thermophilum* (39,40). However, in a previous study, the Suz12 homolog was found to be absent in the yeast *Cryptococcus neoformans*, where two novel PRC2 subunits Bnd1 and Ccc1, may be functional homologs of Suz12 (41). In agreement with previous findings in *Neurospora*, we found that homologs of Ezh2, Eed and Suz12 are core components of PRC2 in *F. graminearum*, and depletion of these three core subunits led to elimination of H3K27me3. The homolog of subunit Nurf55 (FGSG_16720) was not involved in H3K27me3 deposition in *F. graminearum*, although the predicted functional domains of FGSG_16720 were largely intact. Our results were also consistent with the PRC2 function of PRC2 complex in fungal growth and virulence as well as regulating secondary metabolite gene expression in *F. graminearum*, as reported by Freitag's group (32,34). Considering the limited literature and bioinformatic analysis available to date, we propose that the fungal PRC2 components vary significantly, similar to their diver-

sity in plants and animals, while the core Ezh2-Eed-Suz12 module of PRC2 is conserved in fungi.

In plants and animals, H3K27me3 is recognized by specific readers, and then various components of the nuclear signaling network are recruited to repress gene transcription. Many specific domain-containing proteins have been previously found to be involved in H3K27me3 readouts, including PRC1-dependent or PRC1-independent proteins (42). Recent studies indicated that two BAH domain-containing proteins in Arabidopsis, SHL and EBS, interact with the PRC1 component EMF1 to form a BAH-EMF1 complex that then reads the H3K27me3 mark and mediates gene repression in plants (22–24). Recently, another BAH protein in Arabidopsis, AIPP3, coordinates with PHD proteins to read H3K27me3 and unmodified H3K4 and promotes transcriptional repression through dephosphorylation of Pol II (43). However, the mechanism underlying the interpretation of H3K27me3 in fungi remains unclear (7,34). In this study, we found that the BAH-PHD-containing protein BP1 is a methylated H3K27 reader in *F. graminearum*. BP1 directly binds the methylated H3K27 as modified by PRC2 and plays a critical role in gene repression. Consistent with our results, a BAH-PHD-containing protein EPR-1 in *N. crassa* was very recently identified by others as an effector of PRC2, although the binding affinity of EPR-1 for methylated H3K27and its interaction with PRC2 were not investigated. Previously, EPR-1 and H3K27me3 were found to co-occupy and repress an overlapping set of PRC2 target genes (13). In contrast to the SHL and EBS which function depending on PRC1 in plants, BP1 interacts with the PRC2 core component Suz12 directly, which provides a novel pattern of interaction between a reader and PRC2 due to the absence of PRC1 in fungi.

In contrast to other modifications, methylation does not change the overall charge of a histone and thus is unable to directly affect chromatin folding (44). Readers recognize specific histone methylation and recruit other proteins that are essential for chromatin structural changes and subsequent biological outcomes (42). Interestingly, an increasing number of histone readers and associated proteins exhibit nucleic acid-binding activity, which leads to increased affinity for nucleosomes through multivalent contacts. DNA-binding activity ultimately ensures the proper spatial and temporal control of chromatin structure and all DNA-templated processes (36). Currently, the PHD finger, PWWP, chromodomain and Tudor families of histone methylation reader domains are known to possess the ability to bind nucleic acids (36). Among these domains, chromobox 2 (CBX2), a component of PRC1, was shown to bind both H3K27me3 and nucleic acids (45). In addition, the PRC2 accessory protein PHF1 binds DNA and prolongs the residence time of PHF1-PRC2 on chromatin, resulting in more efficient H3K27 methylation (46). In this study, we found that the identified H3K27-methylation reader in *F. graminearum*, BP1, has the DNA-binding activity largely dependent on its PHD finger, which might also contribute to nucleosome occupancy at PRC2 target regions, similar to PHF1 (46). To test this hypothesis, we performed MNase-qPCR to examine nucleosome positioning and occupancy in the genomic regions of the target gene Fg00012 in the wild-type, Δ*Suz12,* Δ*BP1* and ΔΔ*BP1*/*Suz12* double mutant strains (Supplementary Figure S11A). Nucleosome-depleted regions immediately upstream of the transcription start site (TSS) are common in eukaryote promoters (47). The Fg00012 genomic region from −200 to 700 bp was selected for detection. Three well-positioned nucleosomes were identified in the targeted region in the wild type. Nucleosome occupancy was only slightly reduced in Δ*Suz12*; however, we reproducibly found a dramatic reduction (50%) in nucleosome occupancy in the Δ*BP1* strain and a more severe reduction in the double mutant (Supplementary Figure S11B). Consistent with the nucleosome occupancy data, deletion of BP1 led to 50-fold overexpression of Fg00012 compared to that of the wild type. Moreover, the expression level of Fg00012 was significantly higher in the double mutant (ΔΔ*BP1*/*Suz12*) than in the single mutant strains (Supplementary Figure S11C). These results indicate that the DNA-binding activity of BP1 might increase nucleosome residence at H3K27me3-marked genomic regions to reinforce gene transcriptional repression, although additional targeted genes remain to be further investigated.

Unexpectedly, deletion of BP1 did not obviously alter the H3K27me3 levels, although the transcription of PRC2-repressed genes was largely relieved in the Δ*BP1* strain. A similar observation was reported for *N. crassa*: loss of the PRC2 effector EPR-1 derepressed H3K27-methylated genes without loss of H3K27 methylation (13). These observations stand in contrast to findings in plants and animals, in which readers or accessories, such as SHL, EBS and PHF1, positively contribute to the activity of PRC2 (22,46). Given that BP1 has dual binding affinity for methylated H3K27 and DNA and is essential for nucleosome occupancy, a reasonable explanation for the gene repression of BP1 without affecting H3K27 methylation is that PRC2 complex first methylate H3K27 on the target regions, and then, the downstream reader BP1 recognizes and binds methylated H3K27. In addition, BP1 binds DNA to effectively increase nucleosome residence and might reinforce transcriptional repression. The BP1 deletion mutant showed dramatic elimination of nucleosomes from target regions and a loosened chromosome structure, which activates gene transcription, but showed no or a limited effect on the previously methylated histone, since BP1 acts as a downstream effector. Notably, other unidentified accessories of the nuclear signaling network may also participate in this process, such as Rpd3, a histone deacetylase. Rpd3 is important for gene transcriptional repression, and in this study, it was captured by PRC2 components in *F. graminearum*, making it worthy of further investigation.

Studies on PRC2-mediated H3K27 methylation in fungi are increasing rapidly. For example, fungal PRC2 was previously suggested to play important roles in growth, the stress responses, fungus−plant interactions and regulation of secondary metabolites (SMs) (7,34). H3K27me3 modulated the cellular response to genotoxic stress in *N. crassa* (48). In the phytopathogenic fungus *Magnaporthe oryzae*, disruption of the H3K27 methyltransferase MoKMT6 resulted in a slight growth defect but showed significantly attenuated virulence *in planta* (49). H3K27me3 also repressed fungal alkaloid biosynthesis and regulated the normal sym-

biotic interaction between the host plant *Lolium perenne* in symbiotic fungus *Epichloe festucae* (50). In *Fusarium fujikuroi*, deletion of H3K27 methyltransferase Kmt6 was lethal, and knock-down of Kmt6 led to defects in mycelial growth, but increased biosynthesis of SMs (51). In addition, H3K27me3 is reported to regulate the polyketide mycotoxin, dothistromin, in the forest pathogen *Dothistroma septosporum* (52). Consistent with a previous study (32), disruptive mutants of PRC2 core component function and the reader BP1 caused dramatic growth reduction and virulence in *F. graminearum* in our study. In addition, in the present study, BP1 and H3K27me3 were predominately enriched in subtelomeric regions and subsequently played a similar role in the transcriptional repression of SM genes. SM genes encoding PKS, NRPS and cytochrome P450 enzymes (32,35,53) were significantly up-regulated in the mutants. Since some SMs have bioactivity against microbes and deletion mutants of PKS showed increased growth rates in previous studies (53,54), we speculate that enhanced accumulation of SMs produced in the PRC2 and BP1 mutants was one of the reasons for their reduced growth. In contrast to transcriptomic data obtained under low- and high- nitrogen conditions previously identified (32), we found that Kmt6 not only repressed SM genes but was also involved in primary metabolism, such as amino acid and carbon metabolism, when the fungus was grown in YEPD medium. These findings imply that target genes of PRC2 are dynamic and that their growth is condition-dependent. Taken together, the data show that PRC2 and related readers are critical for fungal growth, survival and interkingdom interactions.

Rapid advances in chemical biology and epigenetics are facilitating exploration of targeting the epigenetic machinery, yielding epigenetic therapies for cancer and various human diseases (55–57). Several small-molecule modulators targeting epigenetic machinery or epigenome readers are being screened, and some of these inhibitors have been approved or are in clinical stage trials (57–60). The novel methylated H3K27 reader, BP1, plays important roles in fungal growth and pathogenicity, as well as the expression of secondary metabolite biosynthetic genes in *F. graminearum*, and its orthologs are widely distributed in ascomycetes. Therefore, it is plausible that compounds actively targeting BP1 can be used for plant fungal disease management, especially diseases caused by *Fusarium* species.

DATA AVAILABILITY

Raw data and processed information of the ChIPseq and RNA-seq experiments generated in this article were deposited in the National Center for Biotechnology Information under the accession number PRJNA663410. The mass spectrometry proteomics data have been deposited to the ProteomeXchange Consortium (http://proteomecentral.proteomexchange.org) with the dataset identifier PXD028134.

SUPPLEMENTARY DATA

Supplementary Data are available at NAR Online.

ACKNOWLEDGEMENTS

We are grateful to Mr Chao Liu and Professor Xing-Xing Shen for analyzing RNA-seq data and BP1 ortholog distribution.

Author contributions: Y.C., Z.M. and W.L. conceived the study and supervised the project. G.T. and J.W. designed and performed most of experiments. J.Y. performed protein purification and ITC assays. Y.Z and S.X. performed EMSA experiments. H.W. performed fungal pathogenesis assay. Y.C., Z.M., W.L., C.D., G.T., Z.T., H.L., H.K. and Y.Z. analyzed the study data and wrote the manuscript. All the authors discussed the results and commented on the manuscript.

FUNDING

National Natural Science Fund [31922074, 31930088]; Key Technology R&D Program of Zhejiang Province [2019C02034]; China Agriculture Research System [CARS-3-29]; Fundamental Research Funds for the Central Universities [2021FZZX001-31]. Funding for open access charge: National Natural Science Fund [31922074].

Conflict of interest statement. None declared.

REFERENCES

1. Binder,H., Steiner,L., Przybilla,J., Rohlf,T., Prohaska,S. and Galle,J. (2013) Transcriptional regulation by histone modifications: towards a theory of chromatin re-organization during stem cell differentiation. *Phys. Biol.*, **10**, 026006.
2. Bannister,A.J. and Kouzarides,T. (2011) Regulation of chromatin by histone modifications. *Cell Res.*, **21**, 381–395.
3. Margueron,R. and Reinberg,D. (2011) The Polycomb complex PRC2 and its mark in life. *Nature*, **469**, 343–349.
4. Lewis,E.B. (1978) A gene complex controlling segmentation in *Drosophila*. *Nature*, **276**, 565–570.
5. Simon,J.A. and Kingston,R.E. (2009) Mechanisms of polycomb gene silencing: knowns and unknowns. *Nat. Rev. Mol. Cell Biol.*, **10**, 697–708.
6. Nekrasov,M., Wild,B. and Muller,J. (2005) Nucleosome binding and histone methyltransferase activity of *Drosophila* PRC2. *EMBO Rep.*, **6**, 348–353.
7. Lewis,Z.A. (2017) Polycomb group systems in fungi: new models for understanding polycomb repressive complex 2. *Trends Genet.*, **33**, 220–231.
8. Grau,D.J., Chapman,B.A., Garlick,J.D., Borowsky,M., Francis,N.J. and Kingston,R.E. (2011) Compaction of chromatin by diverse Polycomb group proteins requires localized regions of high charge. *Genes Dev.*, **25**, 2210–2221.
9. Schwartz,Y. and Pirrotta,V. (2007) Polycomb silencing mechanisms and the management of genomic programmes. *Nat. Rev. Genet.*, **8**, 9–22.
10. Blackledge,N.P., Rose,N.R. and Klose,R.J. (2015) Targeting Polycomb systems to regulate gene expression: modifications to a complex story. *Nat. Rev. Mol. Cell Biol.*, **16**, 643–649.
11. Klauke,K., Radulovic,V., Broekhuis,M., Weersing,E., Zwart,E., Olthof,S., Ritsema,M., Bruggeman,S., Wu,X.D., Helin,K. *et al.* (2013) Polycomb Cbx family members mediate the balance between haematopoietic stem cell self-renewal and differentiation. *Nat. Cell Biol.*, **15**, 353–362.
12. Derkacheva,M., Steinbach,Y., Wildhaber,T., Mozgova,I., Mahrez,W., Nanni,P., Bischof,S., Gruissem,W. and Hennig,L. (2013) *Arabidopsis* MSI1 connects LHP1 to PRC2 complexes. *EMBO J.*, **32**, 2073–2085.
13. Wiles,E.T., McNaught,K.J., Kaur,G., Selker,J.M.L., Ormsby,T., Aravind,L. and Selker,E.U. (2020) Evolutionarily ancient BAH-PHD protein mediates Polycomb silencing. *Proc. Natl. Acad. Sci. U. S. A.*, **117**, 11614–11623.
14. Liang,S.C., Hartwig,B., Perera,P., Mora-Garcia,S., de Leau,E., Thornton,H., de Lima Alves,F., Rappsilber,J., Yang,S., James,G.V.

et al. (2015) Kicking against the PRCs - a domesticated transposase antagonises silencing mediated by Polycomb group proteins and is an accessory component of Polycomb repressive complex 2. *PLoS Genet.*, **11**, e1005660.
15. Blackledge,N.P., Farcas,A.M., Kondo,T., King,H.W., McGouran,J.F., Hanssen,L.L.P., Ito,S., Cooper,S., Kondo,K., Koseki,Y. *et al.* (2014) Variant PRC1 complex-dependent H2A ubiquitylation drives PRC2 recruitment and polycomb domain formation. *Cell*, **157**, 1445–1459.
16. Roure,V. and Bantignies,F. (2009) Polycomb group-mediated gene silencing mechanisms: stability versus flexibility. *Epigenomics*, **1**, 301–318.
17. Kouzarides,T. (2007) Chromatin modifications and their function. *Cell*, **128**, 693–705.
18. Hyun,K., Jeon,J., Park,K. and Kim,J. (2017) Writing, erasing and reading histone lysine methylations. *Exp. Mol. Med.*, **49**, e324.
19. Zhao,D., Zhang,X.J., Guan,H.P., Xiong,X.Z., Shi,X.M., Deng,H.T. and Li,H.T. (2016) The BAH domain of BAHD1 is a histone H3K27me3 reader. *Protein Cell*, **7**, 222–226.
20. Bierne,H., Tham,T.N., Batsche,E., Dumay,A., Leguillou,M., Kerneis-Golsteyn,S., Regnault,B., Seeler,J.S., Muchardt,C., Feunteun,J. *et al.* (2009) Human BAHD1 promotes heterochromatic gene silencing. *Proc. Natl. Acad. Sci. U.S.A.*, **106**, 13826–13831.
21. Kycia,I., Kudithipudi,S., Tamas,R., Kungulovski,G., Dhayalan,A. and Jeltsch,A. (2014) The tudor domain of the PHD finger protein 1 is a dual reader of lysine trimethylation at lysine 36 of histone H3 and lysine 27 of histone variant H3t. *J. Mol. Biol.*, **426**, 1651–1660.
22. Li,Z., Fu,X., Wang,Y., Liu,R. and He,Y. (2018) Polycomb-mediated gene silencing by the BAH–EMF1 complex in plants. *Nat. Genet.*, **50**, 1254–1261.
23. Qian,S., Lv,X., Scheid,R.N., Lu,L., Yang,Z., Chen,W., Liu,R., Boersma,M.D., Denu,J.M. and Zhong,X. (2018) Dual recognition of H3K4me3 and H3K27me3 by a plant histone reader SHL. *Nat. Commun.*, **9**, 2425.
24. Yang,Z., Qian,S., Scheid,R.N., Lu,L., Chen,X., Liu,R., Du,X., Lv,X., Boersma,M.D. and Scalf,M. (2018) EBS is a bivalent histone reader that regulates floral phase transition in Arabidopsis. *Nat. Genet.*, **50**, 1247–1253.
25. Yu,J.-H., Hamari,Z., Han,K.-H., Seo,J.-A., Reyes-Domínguez,Y. and Scazzocchio,C. (2004) Double-joint PCR: a PCR-based molecular tool for gene manipulations in filamentous fungi. *Fungal Genet. Biol.*, **41**, 973–981.
26. Yu,F., Gu,Q., Yun,Y., Yin,Y., Xu,J.R., Shim,W.B. and Ma,Z. (2014) The TOR signaling pathway regulates vegetative development and virulence in *Fusariumgraminearum*. *New Phytol.*, **203**, 219–232.
27. Tao,W.A., Wollscheid,B., O'Brien,R., Eng,J.K., Li,X.J., Bodenmiller,B., Watts,J.D., Hood,L. and Aebersold,R. (2005) Quantitative phosphoproteome analysis using a dendrimer conjugation chemistry and tandem mass spectrometry. *Nat. Methods*, **2**, 591–598.
28. Tang,G., Chen,Y., Xu,J.R., Kistler,H.C. and Ma,Z. (2018) The fungal myosin I is essential for *Fusarium* toxisome formation. *PLoS Pathog.*, **14**, e1006827.
29. Jiang,J., Liu,X., Yin,Y. and Ma,Z. (2011) Involvement of a velvet protein FgVeA in the regulation of asexual development, lipid and secondary metabolisms and virulence in *Fusariumgraminearum*. *PLoS One*, **6**, e28291.
30. Nasmith,C.G., Walkowiak,S., Wang,L., Leung,W.W., Gong,Y., Johnston,A., Harris,L.J., Guttman,D.S. and Subramaniam,R. (2011) Tri6 is a global transcription regulator in the phytopathogen *Fusariumgraminearum*. *PLoS Pathog.*, **7**, e1002266.
31. Kaster,M. and Laubinger,S. (2016) Determining nucleosome position at individual loci after biotic stress using MNase-qPCR. *Methods Mol. Biol.*, **1398**, 357–372.
32. Connolly,L.R., Smith,K.M. and Freitag,M. (2013) The *Fusariumgraminearum* histone H3K27 methyltransferase KMT6 regulates development and expression of secondary metabolite gene clusters. *PLos Genet.*, **9**, e1003916.
33. Zhao,S., Zhang,B., Yang,M., Zhu,J. and Li,H. (2018) Systematic profiling of histone readers in *Arabidopsis thaliana*. *Cell Rep.*, **22**, 1090–1102.
34. Ridenour,J.B., Moller,M. and Freitag,M. (2020) Polycomb repression without bristles: facultative heterochromatin and genome stability in fungi. *Genes (Basel)*, **11**, 638.
35. Sieber,C.M., Lee,W., Wong,P., Münsterkötter,M., Mewes,H.-W., Schmeitzl,C., Varga,E., Berthiller,F., Adam,G. and Güldener,U. (2014) The *Fusariumgraminearum* genome reveals more secondary metabolite gene clusters and hints of horizontal gene transfer. *PLoS One*, **9**, e110311.
36. Weaver,T.M., Morrison,E.A. and Musselman,C.A. (2018) Reading more than histones: the prevalence of nucleic acid binding among reader domains. *Molecules*, **23**, 2614.
37. Bailey,T.L., Boden,M., Buske,F.A., Frith,M., Grant,C.E., Clementi,L., Ren,J.Y., Li,W.W. and Noble,W.S. (2009) MEME SUITE: tools for motif discovery and searching. *Nucleic. Acids. Res.*, **37**, W202–W208.
38. Mozgova,I., Kohler,C. and Hennig,L. (2015) Keeping the gate closed: functions of the polycomb repressive complex PRC2 in development. *Plant J.*, **83**, 121–132.
39. Jiao,L. and Liu,X. (2015) Structural basis of histone H3K27 trimethylation by an active polycomb repressive complex 2. *Science*, **350**, aac4383.
40. Jamieson,K., Rountree,M.R., Lewis,Z.A., Stajich,J.E. and Selker,E.U. (2013) Regional control of histone H3 lysine 27 methylation in *Neurospora*. *Proc. Natl. Acad. Sci. U.S.A.*, **110**, 6027–6032.
41. Dumesic,P.A., Homer,C.M., Moresco,J.J., Pack,L.R., Shanle,E.K., Coyle,S.M., Strahl,B.D., Fujimori,D.G., Yates,J.R. 3rd and Madhani,H.D. (2015) Product binding enforces the genomic specificity of a yeast polycomb repressive complex. *Cell*, **160**, 204–218.
42. Musselman,C.A., Lalonde,M.E., Cote,J. and Kutateladze,T.G. (2012) Perceiving the epigenetic landscape through histone readers. *Nat. Struct. Mol. Biol.*, **19**, 1218–1227.
43. Zhang,Y.Z., Yuan,J., Zhang,L., Chen,C., Wang,Y., Zhang,G., Peng,L., Xie,S.S., Jiang,J., Zhu,J.K. *et al.* (2020) Coupling of H3K27me3 recognition with transcriptional repression through the BAH-PHD-CPL2 complex in *Arabidopsis*. *Nat. Commun.*, **11**, 6212.
44. Martin,C. and Zhang,Y. (2005) The diverse functions of histone lysine methylation. *Nat. Rev. Mol. Cell. Biol.*, **6**, 838–849.
45. Kawaguchi,T., Machida,S., Kurumizaka,H., Tagami,H. and Nakayama,J.I. (2017) Phosphorylation of CBX2 controls its nucleosome-binding specificity. *J. Biochem.*, **162**, 343–355.
46. Choi,J., Bachmann,A.L., Tauscher,K., Benda,C., Fierz,B. and Muller,J. (2017) DNA binding by PHF1 prolongs PRC2 residence time on chromatin and thereby promotes H3K27 methylation. *Nat. Struct. Mol. Biol.*, **24**, 1039–1047.
47. Yen,K.Y., Vinayachandran,V., Batta,K., Koerber,R.T. and Pugh,B.F. (2012) Genome-wide nucleosome specificity and directionality of chromatin remodelers. *Cell*, **149**, 1461–1473.
48. Basenko,E.Y., Sasaki,T., Ji,L.X., Prybol,C.J., Burckhardt,R.M., Schmitz,R.J. and Lewis,Z.A. (2015) Genome-wide redistribution of H3K27me3 is linked to genotoxic stress and defective growth. *Proc. Natl Acad. Sci. U.S.A.*, **112**, E6339–E6348.
49. Pham,K.T., Inoue,Y., Vu,B.V., Nguyen,H.H., Nakayashiki,T., Ikeda,K. and Nakayashiki,H. (2015) *MoSET1* (histone H3K4 methyltransferase in *Magnaportheoryzae*) regulates global gene expression during infection-related morphogenesis. *PLos Genet.*, **11**, e1005385.
50. Chujo,T. and Scott,B. (2014) Histone H3K9 and H3K27 methylation regulates fungal alkaloid biosynthesis in a fungal endophyte-plant symbiosis. *Mol. Microbiol.*, **92**, 413–434.
51. Studt,L., Rosler,S.M., Burkhardt,I., Arndt,B., Freitag,M., Humpf,H.U., Dickschat,J.S. and Tudzynski,B. (2016) Knock-down of the methyltransferase Kmt6 relieves H3K27me3 and results in induction of cryptic and otherwise silent secondary metabolite gene clusters in *Fusariumfujikuroi*. *Environ. Microbiol.*, **18**, 4037–4054.
52. Chettri,P., Dupont,P.Y. and Bradshaw,R.E. (2018) Chromatin-level regulation of the fragmented dothistromin gene cluster in the forest pathogen *Dothistromaseptosporum*. *Mol. Microbiol.*, **107**, 508–522.
53. Gaffoor,I., Brown,D.W., Plattner,R., Proctor,R.H., Qi,W.H. and Trail,F. (2005) Functional analysis of the polyketide synthase genes in the filamentous fungus *Gibberellazeae* (Anamorph *Fusariumgraminearum*). *Eukaryot Cell*, **4**, 1926–1933
54. Mentges,M., Glasenapp,A., Boenisch,M., Malz,S., Henrissat,B., Frandsen,R.J.N., Guldener,U., Munsterkotter,M., Bormann,J., Lebrun,M.H. *et al.* (2020) Infection cushions of *Fusariumgraminearum* are fungal arsenals for wheat infection. *Mol Plant Pathol*, **21**, 1070–1087.

55. Ye,F., Huang,J., Wang,H.B., Luo,C. and Zhao,K.H. (2019) Targeting epigenetic machinery: emerging novel allosteric inhibitors. *Pharmacol. Ther.*, **204**, 107406.
56. Hauser,A.T., Robaa,D. and Jung,M. (2018) Epigenetic small molecule modulators of histone and DNA methylation. *Curr. Opin. Chem. Biol.*, **45**, 73–85.
57. Wimalasena,V.K., Wang,T.J., Sigua,L.H., Durbin,A.D. and Qi,J. (2020) Using chemical epigenetics to target cancer. *Mol. Cell*, **78**, 1086–1095.
58. Ren,C.Y., Morohashi,K., Plotnikov,A.N., Jakoncic,J., Smith,S.G., Li,J.J., Zeng,L., Rodriguez,Y., Stojanoff,V., Walsh,M. *et al.* (2015) Small-molecule modulators of methyl-lysine binding for the CBX7 chromodomain. *Chem. Biol.*, **22**, 161–168.
59. Milosevich,N. and Hof,F. (2016) Chemical inhibitors of epigenetic methyllysine reader proteins. *Biochemistry-Us*, **55**, 1570–1583.
60. Zhu,H.H., Wei,T., Cai,Y. and Jin,J.J. (2020) Small molecules targeting the specific domains of histone-mark readers in cancer therapy. *Molecules*, **25**, 578.